Electronic Supplementary Information

Mechanism of photocatalytic CO_2 methanation on ultrafine Rh nanoparticles

Xinyan Dai and Yugang Sun*
Department of Chemistry, Temple University, 1901 North 13th Street, Philadelphia, Pennsylvania 19122, USA. *e-mail: ygsun@temple.edu

Part I. Experimental Section

Synthesis and functionalization of SiO_x nanospheres

A modified Stöber method was used to synthesize SiO_x nanospheres (NSs) with size of ~400 nm.[1] A mixture containing 29.10 mL of absolute ethanol (Pharmco-Aaper), 3.21 mL of deionized (DI) water and 1.96 mL of ammonia hydroxide (NH_3•H_2O, Fisher Scientific) was prepared in a rounded flask at room temperature. To this solution was then added 1.7 mL of tetraethyl orthosilicate (TEOS, Sigma) while stirring at 600 rpm. The reaction proceeded for 2 hours. The product was collected using centrifugation and washing with ethanol for two times, followed by drying in an oven set at 60 ^oC. The synthesized SiO_x NSs were then functionalized with (3-amniopropyl)triethoxysilane (APTES, Sigma) to introduce positive surface charge. In a typical process, 200 mg of SiO_x NSs were dispersed in 100 mL of 190 proof ethanol in a sonication bath. To this dispersion was added dropwise 1 mL of APTES while maintaining the temperature at 60 ^oC. The reaction lasted 8 hours at 60 ^oC, followed by aging at room temperature overnight. Magnetic stirring was maintained throughout the entire process. The APTES-functionalized SiO_x NSs (APTES-SiO_x) were collected using centrifugation and washing with ethanol for two times. The APTES-SiO_x powder was dried in an oven.

Synthesis of Rh-NP/SiO_x-NS composite catalyst

The Rh-NP/SiO_x-NS composite catalysts with Rh loading content of 2.14 wt.% were prepared via an in-situ reduction method. For the Rh-NP/SiO_x-NS composite with Rh NPs of 2.26 nm in size, 40 mg of APTES-SiO_x powder was dispersed in 8 mL of DI water using sonication. To this

dispersion was added a solution containing 5 mg of sodium hexachlororhodate (III) dodecahydrate (Na_3RhCl_6 •12 H_2O, Alfa Aesar) and 7 mL of DI water. The mixture was stirred for 2 hours to allow adsorption of $RhCl_6^{3-}$ anions on the surface of SiO_x NSs. An aqueous solution of 2 mg·ml^{-1} sodium citrate ($Na_3C_6H_5O_7$ • $2H_2O$, Alfa Aesar) with a volume of 15 mL was then added to the mixture. After stirring for 1 minute, 5 mL aqueous solution of 0.7 mg·ml^{-1} sodium borohydride ($NaBH_4$, Alfa Aesar) was added dropwise using a syringe pump at a speed of 30 mL·h^{-1} when the flask was immersed in an ice-water bath to maintain a temperature of 3 ºC. The color of the solution changed from pink to brownish as more $NaBH_4$ solution was added. After the reaction aged for 2 hours, the product was collected using centrifugation and washing with 50%/50% water/ethanol for three times. The size of Rh NPs was analyzed by measuring the diameter of at least 200 particles for each sample in the transmission electron microscopy (TEM) images via ImageJ software.

For the Rh-NP/SiO_x-NS composites with Rh NPs with average sizes of 1.71 nm and 4.20 nm, the procedure was similar but adjustment of reaction solution and temperature was necessary. In the synthesis of 1.71-nm Rh NPs, 15 mL aqueous solution of 1 mg·ml^{-1} $Na_3C_6H_5O_7$ • $2H_2O$ was used. One mL of 3.5 mg·ml^{-1} $NaBH_4$ aqueous solution was added dropwise using a syringe pump at a speed of 15 mL·h^{-1} when the flask was at room temperature. The loading content of Rh was 1.66 wt.% determined by inductively coupled plasms optical emission spectroscopy (ICP-OES). In the synthesis of Rh NPs with an average size of 4.20 nm, 35 mL of 1 mg·ml^{-1} $Na_3C_6H_5O_7$ • $2H_2O$ was used. One mL of 3.5 mg·ml^{-1} $NaBH_4$ aqueous solution was added dropwise using a syringe pump at a speed of 15 mL·h^{-1} when the flask was immersed in an ice-water bath to maintain a temperature of 3 ºC. The loading content of Rh was 1.68 wt.% determined by ICP-OES.

Synthesis of Rh NPs on Al_2O_3 nanoparticles

The procedure was the same as the synthesis of Rh-NP/SiO_x-NS composite with the Rh NPs of 2.26 nm in size. The γ-Al_2O_3 powder was purchased from Alfa Aesar.

Synthesis of Rh NPs on mesoporous silica nanoparticles

Synthesis of mesoporous silica nanoparticles (MSN) was performed by following the method reported in previous study.[2] In a typical synthesis, 1.74 g of NaOH and 10.2 g of potassium phosphate monobasic (KH_2PO_4, Fisher Scientific) were dissolved in 1.5 L of DI H_2O. To this

solution was added 18.55 g of cetrimonium bromide (CTAB, Chem-Impex). The mixture was stirred for one hour until CTAB was completely dissolved. To this solution was added 9.25 mL of TEOS, and the solution was continuously stirred for 12 hours at room temperature. The product was collected through centrifugation and then re-dispersed in 1 vol.% HCl/ethanol solution while maintaining stirring for 12 hours at 60 ^{o}C. Several cycles of centrifuge and washing with water/ethanol were applied to wash trapped CTAB out, forming mesoporous silica nanoparticles. MSNs were further functionalized with APTES as the following process. 140 mg of MSNs was re-dispersed in 270 mL of ethanol in a sonication bath. 0.7 mL of APTES was dropwise added to the dispersion. The reaction lasted three days at 30 ^{o}C. The APTES-functionalized MSNs was washed by twice cycles of centrifugation and washing with ethanol. Loading Rh NPs onto the MSNs was performed by following the procedures of synthesizing the Rh-NP/SiO_x-NS composite with 2.26-nm Rh NPs.

Synthesis of Ag-NP/SiO_x-NS composite

The procedure is modified based on that for preparing Rh-NP/SiO_x-NS composite with 2.26-nm Rh NPs. In the process, 7 mL of aqueous solution containing 1 mg·ml^{-1} silver nitrate ($AgNO_3$, Sigma-Aldrich) and 15 mL of aqueous solution containing 4 mg·ml^{-1} $Na_3C_6H_5O_7 \bullet 2H_2O$ were added to the dispersion of SiO_x NSs. Five mL of 0.175 mg·ml^{-1} $NaBH_4$ aqueous solution was then added using a syringe pump at a speed of 30 mL·h^{-1} when the flask was at room temperature.

Photocatalysis of CO_2 hydrogenation

Photocatalytic CO_2 hydrogenation was conducted in a fixed-bed reactor (Harrick, HVC-MRA-5) equipped with a quartz window. Operating temperature was controlled by a temperature controller kit (Harrick, ATK-024-3) with a thermocouple embedded behind the reaction chamber. Cooling water and a fan were continuously running around the reaction chamber to mitigate heating from the light illumination. Seven mg of catalysts were loaded into a sample cup (6 mm diameter) in the reaction chamber, forming a catalyst bed with a thickness of ~0.7 mm on a platinum grid. Flow rates of gases (Airgas) were controlled using mass flow controllers (Alicat). Catalysts were treated with 10% H_2/Ar gas flow with a flow rate of 17 mL·min^{-1} at 330 ^{o}C for 3 hours prior to reactions. Visible light-driven reactions were conducted with a xenon light source (Asahi Spectra, MAX-303) that was equipped with filters to filter out ultraviolet (UV) irradiation

from the output. Light power intensity was measured with an optical energy meter console (Thorlabs, PM100D) coupled with a thermal sensor head (Thorlabs, S305C). Exit gases were analyzed using a gas chromatography (GC) system equipped with a Carboxen 1010 Plot capillary column (Agilent). Only CO and CH_4 products were detected in this study. The amounts of remaining CO_2, CH_4 product, and CO product were quantified by plugging their GC peak areas into standard linear equations, which were obtained by fitting results of known concentrations of standard gases (Scott) and their GC peak areas. The production rate of a gas species was obtained by multiplying its mole fraction [i.e., moles of the product/(moles of all products + moles of remaining CO_2)] with the CO_2 flow rate. After collecting each data set, the catalysts were re-reduced by hydrogen and tested by carbon dioxide hydrogenation at 330 ^oC under dark conditions to guarantee the catalytic activities were not changed obviously. The deviation of rates for each condition is minimal, and the error bars were not included in the plots for visual clarity if there is no specific note. The error bars in experiments refer to repeated experiments with different batches of catalysts.

DRIFT spectroscopy characterization

Catalyst samples were packed into the high-temperature reaction chamber of a Praying Mantis reactor (ZnSe windows, Harrick) coupled with an infrared absorption spectrometer (Thermo Scientific Nicolet iS35 FT-IR). Gases were flowed to the reaction chamber through Alicat mass flow controllers. Each spectrum was obtained by averaging 200 sequentially collected scans at a resolution of 4 cm^{-1}. Catalysts were treated with 10% H_2/Ar gas flow with a flow rate of 17 $mL \cdot min^{-1}$ at 330 ^oC for 3 hours prior to reactions. Each DRIFT spectrum was obtained by subtracting the background with pure Ar gas or H_2/Ar gas purging from the spectrum during adsorption or hydrogenation reaction. Light illumination could induce baseline changes, so the background spectra were collected under light illumination for 30 minutes until stabilization. For the study of CO_2 adsorption, purging the chamber with Ar at 330 ^oC for 6 hours completely removed the remaining hydrogen left in the chamber and strongly adsorbed on the Rh surface during pre-treatment.

Materials characterization

A transmission electron microscope (JEOL JEM-1400) was used to image the particle samples. Inductively coupled plasma optical emission spectroscopy (ICP-OES, Thermo Scientific 7000 Series) was used to determine Rh loading contents on oxide supports. Diffuse reflectance spectroscopy (DRS) of powder samples was studied with an ultraviolet-visible (UV–vis) spectrophotometer (Thermo Scientific, Evolution 220) equipped with an integration sphere to exclude the scattering effect of nanoparticles.

Part II. Estimation of Temperature Rise under Gas Flow

The cylinder-shaped catalyst bed is assumed as a spherical shape with an equivalent radius *R* (0.1678 cm) since the temperature distribution can be considered uniform radially and axially, verified by heat transport limitation. It is assumed that all the absorbed light is converted to heat to estimate temperature change over radius and time ($\Delta T(r,t)$). The governing equation for the time-dependent heat transfer can be resolved by Pennes' bio-heat generation model:[3-5] $\rho_{medium} c_{medium} \frac{\partial \Delta T}{\partial t} = \nabla(\lambda_{medium} \nabla(\Delta T)) + Q_s + Q_p$. In a sphereical coordinate, the equation can be re-written as: $\frac{1}{\kappa_{medium}} \frac{\partial \Delta T}{\partial t} = \frac{1}{r^2} \frac{\partial}{\partial r}(r^2 \frac{\partial \Delta T}{\partial r}) - \frac{\Delta T}{\kappa_{medium} \tau_{perfusion}} + \frac{Q_p}{\lambda_{medium}}$. Here, it involves photothermal heat generation per volume of catalyst bed (Q_p, W·m^{-3}), heat loss from convection (Q_s, W·m^{-3}), gas perfusion time constant ($\tau_{perfusion}$, s), and thermal conductivity (λ_{medium}, W·m^{-1}·K^{-1}), mass density (ρ_{medium}, g·m^{-3}), heat capacity (c_{medium}, J·g^{-1}·K^{-1}) and thermal diffusivity ($\kappa_{medium} = \frac{\lambda_{medium}}{\rho_{medium} c_{medium}}$, m^2·s^{-1}) of combined medium (SiO_x substrates and gas mixture). Perfusion time constant is obtained from $\tau_{perfusion} = \frac{1}{\rho_{NP} \omega_{NP}}$, where it includes density of nanoparticles in the catalyst bed (ρ_{NP}, g_{NP}·m^{-3}) and gas flow rate per gram of nanoparticles (ω_{NP}, m^3·g_{NP}^{-1}·s^{-1}). Thermal properties of a single component are obtained from reference.[6] The thermal conductivity of the combined medium is averaged based on the porosity of the pellet ε, silica substrate thermal conductivity λ_{SiO_2}, and averaged gas mixture thermal conductivity $\lambda_{gas\ mixture}$, which is $\lambda_{medium} = (1-\varepsilon) \times \lambda_{SiO_2} + \varepsilon \times \lambda_{gas\ mixture}$. Wilke equation is used to obtain the average thermal conductivity of gas mixture.[7] Mass density of the combined medium is obtained by averaging the density of silica substrate and gas mixture based on mole fractions. Heat capacity of the combined medium is obtained by averaging the silica substrate and gas mixture based on the mass fraction. The mathematical resolution of maximum temperature elevation ($\Delta T(0,\infty)$) at

$r = 0$ and infinite time is: $\Delta T(0,\infty) = \frac{Q_p \kappa_{medium} \tau_{perfusion}}{\lambda_{medium}} - \frac{Q_p \kappa_{medium} \tau_{perfusion}}{\lambda_{medium}}((1 + \frac{R}{\sqrt{\kappa_{medium}\tau_{perfusion}}})e^{-R/\sqrt{\kappa_{medium}\tau_{perfusion}}})$.[3, 4] Plugging parameters in Table S1 gives the maximum temperature rise of ~8 °C.

Part III. Correction of light absorption power intensity and calculation of apparent quantum efficiency (AQE)

AQE is defined as the total number of produced methane molecules (n_{CH4}) over the total number of photons absorbed (n_{photon}) by the catalyst. By taking the methane production rates at 330 °C and an incident light power density of 2.184 W·cm^{-2} as an example, the calculation procedure is described as the following. Photocatalytic methane production rate (corrected by subtracting the rate in the dark from that under photoillumination) at 330 °C is 2480.5 μmol·g_{Rh}^{-1}·s^{-1} using 7.2 mg of 2.14 wt.% Rh-NP/SiO_x-NS catalyst. The number of methane molecules, n_{CH4}, produced in one second is

$$n_{CH_4} = 1\ \text{s} \times \frac{2480\ \mu\text{mol}}{g_{Rh}\ \text{s}} \times 7.2\ \text{mg} \times 2.14\% \times \frac{6.02\times10^{23}}{\text{mol}} = 2.34 \times 10^{17}.$$

Calculation of n_{photon} is complex since the light source is not monochromatic light, and the catalyst bed is as thin as ~0.7 mm, which cannot absorb all incident light. At the same time, the Rh-NP/SiO_x-SP composite catalyst has a strong reflectance (or scattering) phenomenon. It means $I_{incident} = I_{transmittance} + I_{reflectance} + I_{absorption}$. The result measured by the power meter showed that 14% of incident light intensity was transmitted for Rh-NP/SiO_x-NS NSs, 7% for Rh/Al_2O_3, and 0 for Rh/MSN (Figure S7a). The sum of percentages of absorbed and reflectance light intensities over incident light intensity is 86% for the Rh-NP/SiO_x-NS catalyst bed. We further used DRS and xenon light source spectrum to find the portion of absorbed light intensity (Figure S7b). The xenon light source spectrum corresponded to incident light intensity $I_{i,\ incident}$ over scanning wavelength (λ) or photon energy (E_i), in which E_i =1240 eV/λ. DRS spectrum of the Rh-NP/SiO_x-NS catalyst gave information on $F(R_\infty)$. R_∞ and $F(R_\infty)$ are defined as[8]: $R_\infty = \frac{I_{reflectance}}{I_{incident}}$ $F(R_\infty) = \frac{(1-R_\infty)^2}{2R_\infty}$. Therefore, R_∞ over different photon energies can be calculated from the DRS spectrum. Meanwhile, we used enough catalysts to measure the DRS spectrum, in which there is no transmittance. R_∞ is able to reflect absorption light intensity as follows: $I_{i,absorption} =$

$I_{i,incident} - I_{i,reflectance} = (1 - R_\infty) \times I_{i,incident}$. The values of (1-$R_\infty$) and $I_{absorption}$ over photon energy are shown in Figure S7b. Integration was done to find the ratio of total photon energy (multiplication product of photon numbers and photon energy) of absorbed light over that of incident light. Total photon energy is calculated, $E_{total} = \int_{1.5eV}^{4.0\ eV} I_i\, E_i dEi$. Spectra of I_iE_i were obtained by calculation as shown in Figure S7c. The integrated areas for incident and absorption light are 3.623 eV and 2.721 eV, respectively. That means the percentage of absorbed light intensity by the catalyst is 75.1%. Based on the information mentioned before, we can calculate $I_{\text{absorption}}$, $I_{\text{absorption}} = \frac{2.18\ \text{W}}{\text{cm}^2} \times 86\% \times 75.1\% = \frac{1.392\ \text{W}}{\text{cm}^2}$. We could convert $I_{\text{absorption}}$ to actual total absorbed photon energy in one second by considering illuminated areas of 0.2826 cm^2, $I_{\text{absorption}} = 1\text{s} \times \frac{1.392\ \text{W}}{\text{cm}^2} \times 0.2826\ \text{cm}^2 \times \frac{\text{eV}}{1.6\times10^{-19}\ \text{J}} = 2.489 \times 10^{18}\ \text{eV}$. In order to obtain the total absorbed photon number, the absorption spectrum was normalized against the highest point at the photon energy of 2.6216 eV (Figure S7d). Therefore, the total absorbed photon energy = $2.489 \times 10^{18}\ \text{eV} = \int_{1.5\ \text{eV}}^{4.0\ \text{eV}} n_{E_i} E_i dE_i = n_{2.6216\ \text{eV}} \int_{1.5\ \text{eV}}^{4.0\ \text{eV}} I_{\text{normalized absorption}} E_i dE_i = n_{2.6216\ \text{eV}} \times 3.516\ \text{eV}$. Total photon number at 2.6216 eV is equal to 7.08×10^{17}. Finally, total photon number is calculated:

$$n_{total} = n_{2.6216} \int_{1.5\ \text{eV}}^{4.0\ \text{eV}} I_{normalized\ absorption} dE_i = 7.08 \times 10^{17} \times 1.392 = 9.855 \times 10^{17}$$

Finally, the apparent quantum efficiency is:

$$\text{AQE} = \frac{2.3\times10^{17}}{9.855\times10^{17}} \times 100\% = 23.3\%.$$

Part IV. Assessment of Mass and Heat Transportation

Internal and external transfer resistance that can affect the measurement of temperature and reaction kinetics need to be excluded. We found that methanation rates and total CO_2 consumption rates are invariant with the gas flow velocity, the concentration of CH_4, and the total concentration of CH_4 and CO in the effluent, following a linear relationship with gas velocity (Figure S19). It means the external mass transport is negligible. We further used empirical Weisz-Prater[9] and Mears[10] criteria to theoretically assess if mass and heat transport are negligible to allow a deviation of less than 5% between the observed and intrinsic reaction rates and temperature. The parameters

for the calculations are listed in Table S1. Thermal properties of a single component are obtained from reference.[6] Extreme conditions are considered.

Internal mass transport

Weisz-Prater parameter (C_{WP})[9] is calculated to determine if the internal mass transport limits the reaction. If internal mass transport is fast enough, it should meet the criteria: $C_{WP} = \frac{r \times R_P^2}{D_{eff} \times C_s} < 1/n$. Here it involves reaction rate per volume of catalyst pellet (r, mol· m^{-3}·s^{-1}), particle radius (R_p, m), effective diffusivity (D_{eff}, m^2·s^{-1}), surface concentration of the limiting reagent (C_s, mol·m^{-3}) and reaction order (n). The effective diffusivity, D_{eff}, of gas in a catalyst bed is then calculated based on the equation of $D_{\text{eff}} = \frac{D_{AB} \varepsilon \sigma_c}{\tau}$, where includes binary diffusivity of CO_2 in H_2 (D_{AB}, m^2·s^{-1}), pellet tortuosity (τ), pellet constriction factor (σ_c) and pellet porosity (ε). D_{AB} of CO_2 in H_2 is calculated based on the equation by Fuller et al.,[11] $D_{AB} = \frac{10^{-7} T^{1.75} \left[\frac{1}{M_A} + \frac{1}{M_B}\right]^{1/2}}{P({V_A}^{1/3} + {V_B}^{1/3})^2}$. It includes temperature (T, K), molecular mass (M_A and M_B, g·mol^{-1}), pressure (P, atm) and atomic diffusion volume (V_A and V_B). Diffusion volumes of CO_2 and H_2 can be found in the reference.[11] Pellet tortuosity can be estimated based on pellet porosity by $\tau = \frac{1}{\varepsilon}$.[12] C_{WP} is 0.003 for the rapidest reaction rates below 1/n, which means internal mass transport limitation is considered negligible.

External mass transport

Mears criterion[10] was used to determine if external mass transport for an n^{th}-order reaction can be neglected relative to surface reaction: $\frac{r \times R_P}{k \times C_s} < \frac{0.15}{n}$. Here k refers to gas-particle mass transfer coefficient in unit of m·s^{-1}. The calculation of k is based on the Sherwood number, Reynolds number (Re), Schmidt number (Sh), and their correlation reported by Wakao et al.,[13] $Sh = \frac{k \times d_P}{D_{eff}} = 2 + 1.1 \times Re^{0.6} Sc^{1/3} = 2 + 1.1 \times (\frac{\varepsilon \times \boldsymbol{u} \times d_P}{(\pi {R_{tube}}^2) \times \upsilon})^{0.6} (\frac{\upsilon}{D_{eff}})^{1.3}$. Here, it involves total flow rates ($\boldsymbol{u}$, m^3·s^{-1}), inner radius of reactor tube (R_{tube}, m), kinematic viscosity of the mixture (υ, m^2·s^{-1}). Other parameters are the same as those aforementioned. The value of the kinematic viscosity of the gas mixture equals the ratio of the dynamic viscosity of the gas mixture ($\eta_{mixture}$, g·m^{-1}·s^{-1}) to the density of the gas mixture ($\rho_{mixture}$, g·m^{-3}). The dynamic viscosity of the gas mixture is

estimated based on the equation proposed by Wilke et al.,[7] $\eta_{mixture} = \sum_{i=1}^{N} \frac{x_i \eta_i}{\sum_j x_j \varphi_{ij}}$ and $\varphi_{ij} = \frac{(1+(\frac{\eta_i}{\eta_j})^{0.5}(\frac{MW_j}{MW_i})^{0.25})^2}{\sqrt{8(1+\frac{MW_j}{MW_i})}}$. It involves the dynamic viscosity (η_i), mole fraction (x_i) and molecular weight (MW_i) of each species. The calculated result of $\frac{r \times R_P}{k \times C_s}$ is equal to 0.001, which is far below 0.15/n for an n[th]-order reaction. It shows that the reaction of free of external mass transport.

Internal heat transport

Anderson criterion[10] was used to determine whether internal heat transport limits the reaction, which means $\frac{|\Delta H| \times r \times R_P^2}{\lambda_{eff} \times T_s} < \frac{T_s \times R}{E_a}$. Here, it involves reaction enthalpy (ΔH, J·mol^{-1}), effective thermal conductivity of the catalyst pellet (λ_{eff}, W·m^{-1}·K^{-1}), thermodynamic temperature at the catalyst surface (T_s, K), ideal gas constant (R, J·mol^{-1}·K^{-1}), and activation energy (E_a, J·mol^{-1}). The effective thermal conductivity is averaged based on the porosity of the pellet (ε), silica substrate thermal conductivity (λ_{SiO_2}), and averaged gas mixture thermal conductivity ($\lambda_{gas\ mixture}$), and is calculated using $\lambda_{eff} = (1-\varepsilon) \times \lambda_{SiO_2} + \varepsilon \times \lambda_{gas\ mixture}$. $\lambda_{gas\ mixture}$ is estimated based on Wilke equation.[7] The calculated result of $\frac{\Delta H \times r \times R_P^2}{\lambda_{eff} \times T_s}$ is 0.001, which is much smaller than 0.13, the value calculated from $\frac{T_s \times R}{E_a}$. Therefore, internal heat transport inside the catalyst bed is negligible.

External heat transport

Mears criterion[10] was used to determine if external heat transport for an n[th]-order reaction can be neglected relative to the surface reaction. The negligible external heat transport requires $\frac{|\Delta H| \times r \times R_P}{h \times T_b} < \frac{0.15 \times T_b \times R}{E_a}$. Here h refers to the gas-particle heat transfer coefficient in unit of m·s^{-1} and the temperature of the gas bulk adjacent to the catalyst surface (T_b, K). The calculation of h is based on the Nusselt number, Reynolds number, Prandtl number, and their correlation reported by Ranz et al.,[14] $Nu = \frac{h \times d_P}{\lambda_{eff}} = 2 + 1.1 \times Re^{0.6} Pr^{1/3} = 2 + 1.1 \times (\frac{\boldsymbol{u} \times \rho_{mixture} \times d_P}{(\pi {R_{tube}}^2) \times \eta_{mixture}})^{0.6} (\frac{\upsilon}{\kappa_{mixture}})^{1.3}$. Here, it involves the total flow rates ($\boldsymbol{u}$, m^3·s^{-1}), the inner radius of reactor tube (R_{tube}, m^2), the kinematic viscosity of the gas mixture (υ, m^2·s^{-1}), the dynamic viscosity of the gas mixture

($\eta_{mixture}$, g·m^{-1}·s^{-1}), thermal diffusivity of the gas mixture ($\kappa_{mixture}$, m^2·s^{-1}), average density of the gas mixture ($\rho_{mixture}$, g·m^{-3}), and diameter of the catalyst particle (d_P, m). Thermal diffusivity of the gas mixture is calculated as $\kappa_{mixture} = \frac{\lambda_{eff}}{\rho_{mixtrue} C_{mixture}}$, in which $C_{mixture}$ (g·mol^{-1}·K^{-1}) is the average specific heat capacity of the gas mixture estimated based on the volume fraction (x_i) of each component ($C_{p,mixture} = \frac{\sum_i \rho_i x_i C_{p,i}}{\rho_{mixture}}$). The calculated result of $\frac{|\Delta H| \times r \times R_P}{h \times T_b}$ is equal to 0.001, which is much lower than 0.019 calculated from $\frac{0.15 \times T_b \times R}{E_a}$. The comparison indicates that external heat transfer is negligible.

Radial transfer[15]

Radial transfer is significant when the ratio of the radius of the reactor tube to the radius of particle size is below 8.[16] In this work, the ratio is estimated to be larger than 15. Therefore, radial dispersion is considered as negligible. To further assess the radial heat transfer, Mears criterion[10] was used. If the radial temperature distribution is uniform, it requires to meet the inequality of $\frac{|\Delta H| \times r \times (1-\varepsilon) \times R_{tube}^2}{\lambda_{eff} \times T_w} < \frac{0.4 \times T_{tube} \times R}{E_a}$. Here, it involves the inner radius (R_{tube}, m) and temperature (T_{tube}, K) of the reactor tube. The calculated value of the left side is 0.049, which is a bit smaller than the value of the right side (0.050). Fulfilling the inequality means that radial heat transfer is not signficant and the radial temperature distribution is uniform.

Axial mass and heat transfer

Axial dispersion was assessed using the criteria proposed by Young et al.[15] Negligible radial mass transfer requires $\frac{r \times (1-\varepsilon) \times d_P}{\frac{u}{\pi {R_{tube}}^2} \times C_0} \ll Pe_{mass}$. Here, it involves Péclet number for the mass transfer (Pe_{mass}), which can be estimated based on its correlation with the Reynolds number and Schmidt number,[17] $\frac{1}{Pe_{mass}} = \frac{0.3}{Re \times Sc} + \frac{0.5}{1+\frac{3.8}{Re \times Sc}}$. Pe_{mass} is three orders of magnitudes larger than the left side of the inequality in the criterion. Therefore, axial mass transfer should be negligible. Negligible axial heat transfer requires $\frac{|\Delta H| \times r \times (1-\varepsilon) \times d_P}{\frac{u}{\pi {R_{tube}}^2} \times (T_w - T_{inlet}) \times \rho_{mixtrue} \times C_{p,mixture}} \ll Pe_{heat}$. Here, it involves Péclet number for the heat transfer (Pe_{heat}), which is equal to $\frac{\frac{u}{\pi {R_{tube}}^2} \times d_P}{\kappa_{axial}}$. The axial thermal diffusivity

(κ_{axial}, $m^2 \cdot s^{-1}$) is estimated based on the correlation reported by Wakao et al,[13] in which $\kappa_{axial} = \frac{\lambda_{eff}}{\varepsilon \times \rho_{mixtrue} C_{p,mixture}}$. Pe_{heat} is two orders of magnitudes larger than the left side of the inequality in the criterion. Therefore, axial heat transfer should be negligible.

Part V. Derivation of Reaction Mechanism

Over 40 reaction kinetics equations were derived from the reaction mechanisms summarized in Table S3. The possible reaction routes are summarized in 5 categories: (A) CO_2* →CO* →C*, (B) CO_2* →CO* →H_xCO*→CH_x*, (C) CO_2* →HCOO*→CO*→C*, (D) CO_2* →HCOO*→ CO*→HCO*→ C* or CH_x*, and (E) CO_2* →HCOO*→CO*→H_2CO*→ CH_x*. The possible rate-determining steps (RDS) include the direct dissociation of CO*, the formation and hydrogenation of HCO* or H_2CO*, and the hydrogenation of C*. Two examples demonstrate how to derive a methane production rate equation from the proposed mechanism.

The derivation of B1b equation in Table S3 treats step 4 as RDS, step 8 as an irreversible step, and other steps as quasi-equilibrium while assuming H*, HCO* as the most abundant surface intermediates (MASI). The percentage of available surface sites are θ^*. Equation B1b is obtained by following:

$$\theta_{\mathrm{H}^*} = (K_2 P_{\mathrm{H}_2})^{\frac{1}{2}} \theta^*; \qquad \theta_{\mathrm{CO}^*} = \frac{K_1 P_{\mathrm{CO}_2}}{\theta_{\mathrm{O}^*}} \theta^{*2}; \qquad \theta_{\mathrm{HCO}^*} = \frac{K_3 K_1 P_{\mathrm{CO}_2} (K_2 P_{\mathrm{H}_2})^{\frac{1}{2}}}{\theta_{\mathrm{O}^*}} \theta^{*2}; \qquad K_7 \theta_{\mathrm{O}^*} \theta_{\mathrm{H}^*} = \theta_{\mathrm{OH}^*} \theta^*$$

$$2v_{\mathrm{CH}_4} = \frac{2k_4 K_3 K_1 P_{\mathrm{CO}_2} (K_2 P_{\mathrm{H}_2})^{\frac{1}{2}}}{\theta_{\mathrm{O}^*}} \theta^{*3} = v_8 = k_8 \theta_{\mathrm{OH}^*} (K_2 P_{\mathrm{H}_2})^{\frac{1}{2}} \theta^* = k_8 K_7 \theta_{\mathrm{O}^*} (K_2 P_{\mathrm{H}_2})^1 \theta^{*1}$$

$$\theta_{\mathrm{O}^*} = \left(\frac{2k_4 K_3 K_1 P_{\mathrm{CO}_2}}{k_8 K_7 (K_2 P_{\mathrm{H}_2})^{1/2}}\right)^{1/2} \theta^*; \qquad \theta_{\mathrm{HCO}^*} = \frac{(k_8 K_7 k_4 K_3 K_1 P_{\mathrm{CO}_2})^{1/2} (K_2 P_{\mathrm{H}_2})^{3/4}}{(2k_4)^{1/2}} \theta^{*1}$$

$$v_{\mathrm{CH}_4} = \frac{k_4 K_3 K_1 P_{\mathrm{CO}_2} (K_2 P_{\mathrm{H}_2})^{\frac{1}{2}}}{\left(\frac{2k_4 K_3 K_1 P_{\mathrm{CO}_2}}{k_8 K_7 (K_2 P_{\mathrm{H}_2})^{1/2}}\right)^{1/2}} \theta^{*2} = \frac{(k_8 K_7 k_4 K_3 K_1 P_{\mathrm{CO}_2})^{1/2} (K_2 P_{\mathrm{H}_2})^{\frac{3}{4}}}{(2)^{1/2}} \theta^{*2}$$

$$1 = \theta^* + \theta_{\mathrm{CHO}^*} + \theta_{\mathrm{H}^*}; \qquad \theta^* = \frac{1}{1 + (K_2 P_{\mathrm{H}_2})^{\frac{1}{2}} + \frac{(k_8 K_7 k_4 K_3 K_1 P_{\mathrm{CO}_2})^{1/2} (K_2 P_{\mathrm{H}_2})^{3/4}}{(2k_4)^{1/2}}}$$

$$v_{\mathrm{CH}_4} = \frac{(k_8 K_7 k_4 K_3 K_1 P_{\mathrm{CO}_2})^{1/2} (K_2 P_{\mathrm{H}_2})^{\frac{3}{4}}}{(2)^{\frac{1}{2}} \{1 + (K_2 P_{\mathrm{H}_2})^{\frac{1}{2}} + \frac{(k_8 K_7 k_4 K_3 K_1 P_{\mathrm{CO}_2})^{1/2} (K_2 P_{\mathrm{H}_2})^{3/4}}{(2k_4)^{1/2}}\}^2}$$

The derivation of E6a equation in Table S3 assumes step 6 as RDS and other steps as quasi-equilibrium while H_2CO^* and CO^* are considered MASI. Equation E6a is obtained by following:

$$\theta_{H^*} = (K_1 P_{H_2})^{\frac{1}{2}} \theta^*; \qquad \theta_{CO_2{}^*} = K_2 P_{CO_2} \theta^*; \qquad \theta_{H_2O^*} = \frac{P_{H_2O}\theta^*}{K_8};$$

$$\theta_{HCO_2{}^*} = \frac{K_3 \theta_{CO_2{}^*} \theta_{H^*}}{\theta^*} = K_3 (K_2 P_{CO_2})(K_1{}^{0.5} P_{H_2}{}^{0.5}) \theta^*$$

$$\theta_{CO^*} = \frac{K_4 \theta_{HCO_2{}^*} \theta_{H^*}}{\theta_{H_2O^*}} = \frac{K_4\, K_3 K_8 (K_2 P_{CO_2})(K_1 P_{H_2})}{P_{H_2O}} \theta^*; \qquad \theta_{H_2CO^*} = \frac{K_5 \theta_{CO^*} \theta_{H^*}{}^2}{\theta^{*2}} = \frac{K_5 K_3 K_4 K_8 (K_2 P_{CO_2})(K_1{}^2 P_{H_2}{}^2)}{P_{H_2O}} \theta^*$$

$$v_{CH_4} = k_6 \theta_{H_2CO^*} \theta_{H^*}{}^2 = \frac{k_6 K_5 K_3 K_4 K_8 (K_2 P_{CO_2})(K_1 P_{H_2})^3}{P_{H_2O}} \theta^{*3}$$

$$1 = \theta^* + \theta_{CO^*} + \theta_{H_2CO^*}; \theta^* = \frac{1}{1 + \frac{K_4\, K_3 K_8 (K_2 P_{CO_2})(K_1 P_{H_2})}{P_{H_2O}} + \frac{K_5 K_3 K_4 K_8 (K_2 P_{CO_2})(K_1{}^2 P_{H_2}{}^2)}{P_{H_2O}}}$$

$$v_{CH_4} = \frac{k_6 K_5 K_3 K_4 K_8 (K_2 P_{CO_2})(K_1 P_{H_2})^3}{P_{H_2O}\{1 + \frac{K_4\, K_3 K_8 (K_2 P_{CO_2})(K_1 P_{H_2})}{P_{H_2O}} + \frac{K_5 K_3 K_4 K_8 (K_2 P_{CO_2})(K_1{}^2 P_{H_2}{}^2)}{P_{H_2O}}\}^3}$$

When the partial pressures of H_2O and CO_2 are fixed, we can define new constants: $k_1 = \frac{k_6 K_3 K_4 K_5 K_8 (K_2 P_{CO_2}) K_1{}^3}{P_{H_2O}}$; $k_2 = \frac{K_4 K_3 K_8 (K_2 P_{CO_2}) K_1}{P_{H_2O}}$; $k_3 = \frac{K_5 K_3 K_4 K_8 (K_2 P_{CO_2}) K_1{}^2}{P_{H_2O}}$. The methane production rate equation is simplified as $v_{CH_4} = \frac{k_1 \times P_{H_2}{}^3}{(1 + k_2 \times P_{H_2} + k_3 \times P_{H_2}{}^2)^3}$ or $\frac{P_{H_2}}{v_{CH_4}{}^{1/3}} = \frac{1}{k_1{}^{1/3}} + \frac{k_2}{k_1{}^{1/3}} \times P_{H_2} + \frac{k_3}{k^{1/3}} \times P_{H_2}^2$.

Table S1 Parameters used for calculating temperature rise and assessing transport limitation.

Height of catalyst bed (m)	7×10^{-4}
Radius of reactor tube (R_{tube}, m)	3×10^{-3}
Density of nanoparticles in the catalyst bed ($\boldsymbol{\rho}_{NP}$, g•cm^{-3})	7.6×10^{-3}
Gas flow rate per gram of nanoparticles (ω_{NP}, cm^3•g$_{NP}^{-1}$•s^{-1})	1038
Perfusion time constant ($\tau_{perfusion}$, s)	0.1272
Volumetric heat generation rate (Q_p, W•cm^{-3})	21.41
Volume fraction of pores in catalyst bed (ε)	0.8
Gas mixture thermal conductivity ($\lambda_{gas\ mixture}$, W•m^{-1}•K^{-1})	0.0875
Combined medium thermal conductivity λ_{medium}or effective thermal conductivity of the catalyst pellet λ_{eff} (W•m^{-1}•K^{-1})	0.3038
Combined medium density (ρ_{medium}, g•cm^{-3})	0.3540
Combined medium specific heat capacity (c_{medium}, J•g^{-1}•K^{-1})	0.8869
Radius of catalyst particle (R_p, m)	2×10^{-4}
Temperature (T, T_s, T_b, T_w, K)	603.15
Volume or molar fraction of gas species (x_{Ar}, x_{H2}, x_{CO2})	0.1518, 0.7857, 0.0625
Reaction rate per volume of catalysts pellet (r, mol• m^{-3}•s^{-1})	19.81
Binary diffusivity of CO_2 in H_2 (D_{AB}, m^2•s^{-1})	2.34×10^{-4}
Effective diffusivity (D_{eff}, m^2•s^{-1})	1.2×10^{-4}
Surface concentration of the limiting reagent (C_s, mol•m^{-3})	2.555
Total gas flow rates (u, m^3•s^{-1})	9.72×10^{-6}
Dynamic viscosity of the gas mixture ($\eta_{mixture}$, g•m^{-1}•s^{-1})	2.83×10^{-2}
Density of the gas mixture ($\rho_{mixture}$, g•m^{-3})	367
Kinematic viscosity of the gas mixture (υ, m^2•s^{-1})	7.72×10^{-5}
Reynolds number (Re); Schmidt number (Sc); Sherwood number (Sh); Prandtl number (Pr); Nusselt number number (Nu)	1.43;0.33;2.94;0.18; 2.14
Gas-particle mass transfer coefficient (k, m•s^{-1})	1.72
Reaction enthalpy (ΔH,J•mol^{-1})	2.53×10^5
Activation energy (E_a, J•mol^{-1})	4.0×10^4
Thermal diffusivity of the gas mixture ($\kappa_{mixture}$, m^2•s^{-1})	4.33×10^{-4}
Specific heat capacity of gas mixture ($c_{mixture}$, J•g^{-1}•K^{-1})	1.915
Gas-particle heat transfer coefficient (h, m•s^{-1})	1625
Péclet number for the mass transfer (Pe_{mass}) and heat transfer (Pe_{heat})	1.44;0.25
Axial thermal conductivity (κ_{axial}, m^2•s^{-1})	5.41×10^{-4}

Table S2. Summary of FTIR peak assignments.

Sample	Conditions	Assignment/stretching frequency (cm^{-1})	Species	Ref.
SiO_x	CO_2 or CO_2+H_2	ν_{OH} 3747 negative signals	single -OH	18, 19
		$\nu_{as\ O\text{-}C\text{-}O}$ 1678; $\nu_{s\ O\text{-}C\text{-}O}$ 1414	m-HCO_3*	18, 19
		$\nu_{as\ O\text{-}C\text{-}O}$ 1625	bi-HCO_3*	18, 19
		$\nu_{as\ O\text{-}C\text{-}O}$1554; $\nu_{s\ O\text{-}C\text{-}O}$ 1388	bi-CO_3*	18, 19
Rh/SiO_x	CO_2	$\nu_{as\ O\text{-}C\text{-}O}$ 1678; $\nu_{s\ O\text{-}C\text{-}O}$ 1414	m-HCO_3*	18, 19
		$\nu_{as\ O\text{-}C\text{-}O}$ 1625	bi-HCO_3*	18, 19
		$\nu_{as\ O\text{-}C\text{-}O}$1554; $\nu_{s\ O\text{-}C\text{-}O}$ 1388	bi-CO_3*	18, 19
	CO_2+H_2	$\nu_{C\equiv O}$ 2000-2060	L-CO* or carbonyl hydride	**20-23**
		$\nu_{C\equiv O}$ 1910	Brd-CO*	**20-23**
		$\nu_{C\equiv O}$ 1802	Br-CO*	**20-23**
		$\nu_{C\text{-}H}$ 2817, 2708; $\nu_{s\ O\text{-}C\text{-}O}$ 1348	bi-HCOO*	**18, 24-26**
		$\nu_{as\ O\text{-}C\text{-}O}$ 1686	m-HCO_3*	18, 19
		$\nu_{as\ O\text{-}C\text{-}O}$ 1620	bi-HCO_3*	18, 19
	HCOOH	ν_{CH} 2939, 2873; $\nu_{C=O}$ 1741; $\nu_{as\ O\text{-}C\text{-}O}$1589; $\nu_{s\ O\text{-}C\text{-}O}$ 1359	HCOOH (gas)	18, 19
		$\nu_{C\equiv O}$ 2025-2034	L-CO*	**20-23**
		$\nu_{C\equiv O}$ 1902-1924	Brd-CO*	**20-23**
		$\nu_{C\equiv O}$ 1805	Br-CO*	**20-23**
	HCOH (using trioxane as precursor)	ν_{CH2} 2852; $2\omega_{CH2}$ 2789;δ_{CH2} 1470; ω_{CH2} 1410; τ_{CH2} 1310	dioxymethylene $(HCO)_2$	27
		$\nu_{C\equiv O}$ 2000-2060	L-CO or carbonyl hydride	**20-23**
		$\nu_{C\equiv O}$ 1910	Brd-CO*	**20-23**
		$\nu_{C\equiv O}$ 1817	Br-CO*	**20-23**
		$\nu_{as\ CO\text{-}Rh\text{-}CO}$ 2090; $\nu_{s\ CO\text{-}Rh\text{-}CO}$ 2020	gem-dicarbonyl	**20-23**
		$\nu_{C\equiv O}$ 2000-2060	L-CO*	**20-23**
	CO	$\nu_{C\equiv O}$ 1910	Brd-CO*	**20-23**
		$\nu_{C\equiv O}$ 1802	Br-CO*	**20-23**
		$\nu_{C\equiv O}$ 2036	L-CO or rhodium carbonyl hydride	**20-23**
		$\nu_{C\equiv O}$ 1916	Brd-CO*	**20-23**

Table S3 Possible reaction mechanisms and the corresponding methane production rate equations.

A: CO_2* →CO* →C*	
(1) $CO_2 + 2^* \rightleftharpoons CO^* + O^*$ (2) $H_2 + 2^* \rightleftharpoons 2H^*$ (3) $CO^* + ^* \rightleftharpoons C^* + O^*$ (4) $C^* + H^* \rightleftharpoons CH^* + ^*$ (5) $CH^* + 3H^* \rightleftharpoons CH_4^* + 3^*$ (6) $O^* + H^* \rightleftharpoons OH^* + ^*$ (7) $OH^* + H^* \rightleftharpoons H_2O^* + ^*$ (8) $H_2O^* \rightleftharpoons H_2O + ^*$ (9) $CH_4^* \rightleftharpoons CH_4 + ^*$	Step 3 as RDS, step 7 as irreversible, others as quasi-equilibrium; H*, O* and CO* as MASI. $v_{CH_4} = \frac{(\frac{K_1K_2K_6k_3k_7}{2})^{0.5}P_{CO_2}^{0.5}P_{H_2}^{0.5}}{[1+K_2^{0.5}P_{H_2}^{0.5}+(\frac{2K_1k_3}{K_2K_6k_7})^{0.5}(\frac{P_{CO_2}}{P_{H_2}})^{0.5}+(\frac{K_1K_2K_6k_7}{2k_3})^{0.5}P_{CO_2}^{0.5}P_{H_2}^{0.5}]^2}$ (A1a)
	Step 4 as RDS, step 7 as irreversible step, others as quasi-equilibrium; H* and CO* as MASI $v_{CH_4} = \frac{(K_1K_3K_6{}^2k_4k_7{}^2)^{1/3}P_{CO_2}^{1/3}P_{H_2}^{5/6.}}{[1+K_2^{0.5}P_{H_2}^{0.5}+(\frac{K_1{}^2K_6K_2{}^{1/2}k_7}{2k_4K_3})^{1/3}P_{CO_2}^{2/3}P_{H_2}^{1/6}]^2}$ (A1b)
(1) $CO_2 + 2^* \rightleftharpoons CO^* + O^*$ (2) $H_2 + 2^* \rightleftharpoons 2H^*$ (3) $CO^* + ^* \rightleftharpoons C^* + O^*$ (4) $C^* + 2H^* \rightleftharpoons CH_2^* + 2^*$ (5) $CH_2^* + 2H^* \rightleftharpoons CH_4^* + 2^*$ (6) $O^* + H^* \rightleftharpoons OH^* + ^*$ (7) $OH^* + H^* \rightleftharpoons H_2O^* + ^*$ (8) $H_2O^* \rightleftharpoons H_2O + ^*$ (9) $CH_4^* \rightleftharpoons CH_4 + ^*$	Step 4 as RDS, step 7 as irreversible step, others as quasi-equilibrium; H*, O* and CO* as MASI. $v_{CH_4} = \frac{(2k_4K_1K_3P_{CO_2})^{\frac{1}{3}}(k_7K_6)^{\frac{2}{3}}K_2P_{H_2}}{\{1+(K_2P_{H_2})^{\frac{1}{2}}+(\frac{2k_4K_3K_1P_{CO_2}}{k_7K_6})^{\frac{1}{3}}+\frac{(K_1P_{CO_2})^{2/3}(k_7K_6)^{1/3}}{(2k_4K_3)^{1/3}}\}^3}$ (A2)
B: CO_2* →CO* →H_xCO*→CH_x*	
(1) $CO_2 + 2^* \rightleftharpoons CO^* + O^*$ (2) $H_2 + 2^* \rightleftharpoons 2H^*$ (3) $CO^* + H^* \rightleftharpoons HCO^* + ^*$ (4) $HCO^* + ^* \rightleftharpoons CH^* + O^*$ (5) $CH^* + 3H^* \rightleftharpoons CH_4^* + 3^*$ (6) $CH_4^* \rightleftharpoons CH_4 + ^*$ (7) $O^* + H^* \rightleftharpoons OH^* + ^*$ (8) $OH^* + H^* \rightleftharpoons H_2O^* + ^*$ (9) $H_2O^* \rightleftharpoons H_2O + ^*$	Step 3 as RDS, step 8 as irreversible step, others as quasi-equilibrium; H*, CO* as MASI $v_{CH_4} = \frac{(k_3k_8K_7K_1P_{CO_2})^{1/2}(K_2P_{H_2})^{\frac{3}{4}}}{(2)^{\frac{1}{2}}\{1+(K_2P_{H_2})^{\frac{1}{2}}+\frac{(k_8K_7K_1P_{CO_2})^{1/2}\left(K_2P_{H_2}\right)^{\frac{1}{4}}}{(2k_3)^{\frac{1}{2}}}\}^2}$ (B1a)
	Step 4 as RDS, step 8 as irreversible step, others as quasi-equilibrium; H* and HCO* as MASI. $v_{CH_4} = \frac{(k_8K_7k_4K_3K_1P_{CO_2})^{1/2}\,(K_2P_{H_2})^{\frac{3}{4}}}{(2)^{\frac{1}{2}}\{1+(K_2P_{H_2})^{\frac{1}{2}}+\frac{(k_8K_7k_4K_3K_1P_{CO_2})^{1/2}\,(K_2P_{H_2})^{3/4}}{(2k_4)^{1/2}}\}^2}$ (B1b)
(1) $CO_2 + 2^* \rightleftharpoons CO^* + O^*$ (2) $H_2 + 2^* \rightleftharpoons 2H^*$ (3) $CO^* + H^* \rightleftharpoons HCO^* + ^*$ (4) $HCO^* + H^* \rightleftharpoons CH^* + OH^*$ (5) $CH^* + 3H^* \rightleftharpoons CH_4^* + 3^*$ (6) $CH_4^* \rightleftharpoons CH_4 + ^*$ (7) $O^* + H^* \rightleftharpoons OH^* + ^*$ (8) $OH^* + H^* \rightleftharpoons H_2O^* + ^*$ (9) $H_2O^* \rightleftharpoons H_2O + ^*$	Step 4 as RDS, step 8 as irreversible step, others as quasi-equilibrium; H*, O*, CO*, HCO* as MASI. $v_{CH_4} = \frac{(k_8K_7k_4K_3K_1P_{CO_2})^{1/2}\,(K_2P_{H_2})^{1}}{(2)^{\frac{1}{2}}\{1+(K_2P_{H_2})^{\frac{1}{2}}+(\frac{2k_4K_3K_1P_{CO_2}}{k_8K_7})^{\frac{1}{2}}+K_7(\frac{2k_4K_3K_1P_{CO_2}}{k_8K_7})^{1/2}(K_2P_{H_2})^{\frac{1}{2}}\frac{(k_8K_7K_1P_{CO_2})^{\frac{1}{2}}}{(2k_4K_3)^{\frac{1}{2}}}+\frac{(k_8K_3K_7K_1P_{CO_2}K_2P_{H_2})^{1/2}}{(2k_4)^{1/2}}\}^2}$ (B2)
(1) $CO_2 + 2^* \rightleftharpoons CO^* + O^*$ (2) $H_2 + 2^* \rightleftharpoons 2H^*$ (3) $CO^* + H^* \rightleftharpoons HCO^* + ^*$ (4) $HCO^* + 2H^* \rightleftharpoons CH_2^* + OH^* + ^*$ (5) $CH_2^* + 2H^* \rightleftharpoons CH_4^* + 2^*$ (6) $CH_4^* \rightleftharpoons CH_4 + ^*$ (7) $O^* + H^* \rightleftharpoons OH^* + ^*$ (8) $OH^* + H^* \rightleftharpoons H_2O^* + ^*$ (9) $H_2O^* \rightleftharpoons H_2O + ^*$	Step 4 as RDS, step 8 as irreversible step, others as quasi-equilibrium; H*, O*, OH*, CO*, HCO*as MASI. $v_{CH_4} = \frac{(k_8K_7k_4K_3K_1P_{CO_2})^{1/2}\,(K_2P_{H_2})^{1}}{(2)^{\frac{1}{2}}\{1+\left(K_2P_{H_2}\right)^{\frac{1}{2}}+(\frac{2k_4K_3K_1P_{CO_2}}{k_8K_7})^{\frac{1}{2}}\left(K_2P_{H_2}\right)^{\frac{1}{2}}+(\frac{2k_4K_3K_7K_1P_{CO_2}}{k_8})^{1/2}K_2P_{H_2}+\frac{(k_8K_7K_1P_{CO_2})^{1/2}}{(2k_4K_3K_2P_{H_2})^{1/2}}+\frac{(k_8K_3K_7K_1P_{CO_2})^{1/2}}{(2k_4)^{1/2}}\}^3}$ (B3)
(1) $CO_2 + 2^* \rightleftharpoons CO^* + O^*$ (2) $H_2 + 2^* \rightleftharpoons 2H^*$ (3) $CO^* + 2H^* \rightleftharpoons H_2CO^* + 2^*$ (4) $H_2CO^* + ^* \rightleftharpoons CH^* + OH^*$ (5) $CH^* + 3H^* \rightleftharpoons CH_4^* + 3^*$ (6) $O^* + H^* \rightleftharpoons OH^* + ^*$ (7) $OH^* + H^* \rightleftharpoons H_2O^* + ^*$ (8) $H_2O^* \rightleftharpoons H_2O + ^*$ (9) $CH_4^* \rightleftharpoons CH_4 + ^*$	Step 3 as RDS, step 7 as irreversible step, others as quasi-equilibrium; H*, CO* as MASI $v_{CH_4} = \frac{(k_3k_8K_7K_1P_{CO_2})^{1/2}(K_2P_{H_2})^{\frac{3}{4}}}{(2)^{\frac{1}{2}}\{1+(K_2P_{H_2})^{\frac{1}{2}}+\frac{(k_8K_7K_1P_{CO_2})^{1/2}\left(K_2P_{H_2}\right)^{\frac{1}{4}}}{(2k_3)^{\frac{1}{2}}}\}^2}$ (B4a)
	Step 4 as RDS, step 7 as irreversible, others as quasi-equilibrium; CO_2* and H* as MASI. $v_{CH_4} = \frac{K_2(\frac{K_1K_3K_6k_4k_7}{2})^{0.5}P_{CO_2}^{0.5}P_{H_2}}{[1+K_2^{0.5}P_{H_2}^{0.5}+(\frac{K_1K_6k_7}{2K_3k_4})^{0.5}P_{CO_2}^{0.5}]^2}$ (B4b)
	Step 4 as RDS, step 7 as irreversible step, others as quasi-equilibrium; CO_2*, H_2CO*, H* as MASI.

$$v_{CH_4} = \frac{K_2(\frac{K_1K_3K_6k_4k_7}{2})^{0.5}P_{CO_2}^{0.5}P_{H_2}}{[1+K_2^{0.5}P_{H_2}^{0.5}+K_2K_1P_{H_2}P_{CO_2}+(\frac{K_1K_6k_7}{2K_3k_4})^{0.5}P_{CO_2}^{0.5}]^2} \quad \text{(B4c)}$$

Step 3 as RDS, step 7 as irreversible step, others as quasi-equilibrium; H*, O*, OH*, CO*as MASI

(1) $CO_2 + 2^* \rightleftharpoons CO^* + O^*$
(2) $H_2 + 2^* \rightleftharpoons 2H^*$
(3) $CO^* + 2H^* \rightleftharpoons H_2CO^* + 2^*$
(4) $H_2CO^* + H^* \rightleftharpoons CH_2^* + OH^*$
(5) $CH_2^* + 2H^* \rightleftharpoons CH_4^* + 2^*$
(6) $O^* + H^* \rightleftharpoons OH^* + ^*$
(7) $OH^* + H^* \rightleftharpoons H_2O^* + ^*$
(8) $H_2O^* \rightleftharpoons H_2O + ^*$
(9) $CH_4^* \rightleftharpoons CH_4 + ^*$

$$v_{\mathrm{CH_4}} = \frac{(k_7K_6\,k_3K_1P_{\mathrm{CO_2}})^{\frac{1}{2}}(K_2P_{\mathrm{H_2}})^{1}}{(2)^{\frac{1}{2}}\{1+(K_2P_{H_2})^{\frac{1}{2}}+(\frac{2k_3K_1P_{CO_2}}{k_7K_6})^{\frac{1}{2}}+K_6(\frac{2k_3K_2P_{H_2}K_1P_{CO_2}}{k_7K_6})^{\frac{1}{2}}+\frac{(k_7K_6K_1P_{CO_2})^{\frac{1}{2}}}{(2k_3)^{\frac{1}{2}}}\}^3} \quad \text{(B5a)}$$

Step 4 as RDS, step 7 as irreversible, other steps as quasi-equilibrium. H*, O*, OH*, CO*, H_2CO* as MASI.

$$v_{\mathrm{CH_4}} = \frac{(k_7K_6k_4K_3K_1P_{CO_2})^{1/2}\,(K_2P_{H_2})^{5/4}}{(2)^{\frac{1}{2}}\{1+(K_2P_{\mathrm{H_2}})^{\frac{1}{2}}+(\frac{2k_4K_3K_1P_{\mathrm{CO_2}}}{k_7K_6})^{\frac{1}{2}}(K_2P_{\mathrm{H_2}})^{\frac{1}{4}}+(\frac{2k_4K_6K_3K_1P_{\mathrm{CO_2}}}{k_7})^{\frac{1}{2}}(K_2P_{\mathrm{H_2}})^{3/4}+\frac{(k_7K_6K_1P_{\mathrm{CO_2}})^{\frac{1}{2}}}{(2k_4K_3)^{\frac{1}{2}}(K_2P_{\mathrm{H_2}})^{\frac{1}{4}}}+\frac{(k_7K_6K_3K_1P_{\mathrm{CO_2}})^{1/2}(K_2P_{\mathrm{H_2}})^{3/4}}{(2k_4)^{1/2}}\}^2} \quad \text{(B5b)}$$

Step 4 as RDS, step 7 as irreversible, others as quasi-equilibrium; H*, O*, OH*, CO*, H_2CO*, as MASI.

(1) $CO_2 + 2^* \rightleftharpoons CO^* + O^*$
(2) $H_2 + 2^* \rightleftharpoons 2H^*$
(3) $CO^* + 2H^* \rightleftharpoons H_2CO^* + 2^*$
(4) $H_2CO^* + 2H^* \rightleftharpoons CH_3^* + OH^*$
(5) $CH_3^* + H^* \rightleftharpoons CH_4^* + ^*$
(6) $O^* + H^* \rightleftharpoons OH^* + ^*$
(7) $OH^* + H^* \rightleftharpoons H_2O^* + ^*$
(8) $H_2O^* \rightleftharpoons H_2O + ^*$
(9) $CH_4^* \rightleftharpoons CH_4 + ^*$

$$v_{\mathrm{CH_4}} = \frac{(k_7K_6k_4K_3K_1P_{CO_2})^{1/2}(K_2P_{H_2})^{3/2}}{(2)^{\frac{1}{2}}\{1+(K_2P_{H_2})^{\frac{1}{2}}+(\frac{2k_4K_3K_1P_{CO_2}}{k_7K_6})^{\frac{1}{2}}(K_2P_{H_2})^{\frac{1}{2}}+(\frac{2k_4K_6K_3K_1P_{CO_2}}{k_7})^{\frac{1}{2}}K_2P_{H_2}+\frac{(k_7K_6K_1P_{CO_2})^{1/2}}{(2k_4K_3K_2P_{H_2})^{1/2}}+\frac{(k_7K_6K_3K_1P_{CO_2}K_2P_{H_2})^{1/2}}{(2k_4)^{1/2}}\}^3} \quad \text{(B6)}$$

C: CO_2* →HCOO*→CO*→C*

Step 4 as RDS, step 8 as irreversible step and other steps as quasi-equilibrium, H* and CO* as MASI.

(1) $H_2 + 2^* \rightleftharpoons 2H^*$
(2) $CO_2 + H^* \rightleftharpoons HCOO^*$
(3) $HCOO^* + ^* \rightleftharpoons CO^* + OH^*$
(4) $CO^* + ^* \rightleftharpoons C^* + O^*$
(5) $C^* + H^* \rightleftharpoons CH^*$
(6) $CH^* + 3H^* \rightleftharpoons CH_4^* + 3^*$
(7) $O^* + H^* \rightleftharpoons OH^* + ^*$
(8) $OH^* + H^* \rightleftharpoons H_2O^* + ^*$

$$v_{CH_4} = \frac{(k_8k_4K_3K_2P_{CO_2}K_1P_{H_2})^{1/2}}{(2)^{1/2}\{1+(K_1P_{H_2})^{\frac{1}{2}}+\frac{(k_8K_3K_2P_{CO_2}K_1P_{H_2})^{1/2}}{(2k_4)^{1/2}}\}^2} \quad \text{(C1a)}$$

Step 5 as RDS, step 8 as irreversible step, others as quasi-equilibrium; H* and CO* as MASI.

$$v_{CH_4} = \frac{k_5{k_8}^{2/3}(K_7K_4K_3K_2P_{CO_2})^{1/3}(K_1P_{H_2})^{5/6}}{(2k_5)^{2/3}\{1+(K_1P_{H_2})^{\frac{1}{2}}+\frac{{k_8}^{1/2}K_3K_2P_{CO_2}(K_1P_{H_2})^{\frac{1}{2}}}{(2k_4K_3K_2P_{CO_2})^{\frac{1}{2}}}\}^2} \quad \text{(C1b)}$$

(1) $H_2 + 2^* \rightleftharpoons 2H^*$
(2) $CO_2 + H^* \rightleftharpoons HCOO^*$
(3) $HCOO^* + ^* \rightleftharpoons CO^* + OH^*$
(4) $CO^* + ^* \rightleftharpoons C^* + O^*$
(5) $C^* + 2H^* \rightleftharpoons CH_2^*$
(6) $CH_2^* + 2H^* \rightleftharpoons CH_4^* + 2^*$
(7) $O^* + H^* \rightleftharpoons OH^* + ^*$
(8) $OH^* + H^* \rightleftharpoons H_2O^* + ^*$

Step 5 as RDS, step 8 as irreversible step, others as quasi-equilibrium; H* and CO* as MASI.

$$v_{\mathrm{CH_4}} = \frac{(k_5K_7K_4K_2K_3P_{CO_2})^{1/3}(k_8)^{2/3}K_1P_{\mathrm{H_2}}}{(2)^{2/3}\{1+(K_1P_{\mathrm{H_2}})^{\frac{1}{2}}+\frac{({k_8}^{1/2}K_2K_3P_{\mathrm{CO_2}})^{2/3}}{(2k_5K_7K_4)^{1/3}}\}^3} \quad \text{(C2)}$$

Step 5 as RDS, step 8 as irreversible step, others as quasi-equilibrium; H*, CO*, C* as MASI.

(1) $H_2 + 2^* \rightleftharpoons 2H^*$
(2) $CO_2 + H^* \rightleftharpoons HCOO^*$
(3) $HCOO^* + H^* \rightleftharpoons CO^* + H_2O^*$
(4) $CO^* + ^* \rightleftharpoons C^* + O^*$
(5) $C^* + H^* \rightleftharpoons CH^*$
(6) $CH^* + 3H^* \rightleftharpoons CH_4^* + 3^*$
(7) $O^* + H^* \rightleftharpoons OH^* + ^*$
(8) $OH^* + H^* \rightleftharpoons H_2O^* + ^*$
(9) $H_2O^* \rightleftharpoons H_2O + ^*$

$$v_{CH_4} = \frac{(k_5K_9K_2K_3K_4P_{CO_2}k_8)^{1/2}(K_1P_{H_2})^{\frac{5}{4}}}{(2K_7P_{H_2O})^{1/2}\{1+(K_1P_{H_2})^{\frac{1}{2}}+\frac{K_9K_2K_3P_{CO_2}(K_1P_{H_2})^{1}}{P_{H_2O}}+\frac{(K_9K_2K_3K_4P_{CO_2}P_{H_2O}k_8)^{1/2}(K_1P_{H_2})^{\frac{3}{4}}}{P_{H_2O}(2k_5{K_7}^3)^{1/2}}\}^2} \quad \text{(C3)}$$

(1) H_2 + 2* ⇌ 2H*
(2) CO_2 + H* ⇌ HCOO*
(3) HCOO* +H* ⇌ CO*+H_2O*
(4) CO* + * ⇌ C* + O*
(5) C* +2 H* ⇌ CH_2*
(6) CH_2* + 2H* ⇌ CH_4* + 2*
(7) O*+H* ⇌ OH* +*
(8) OH*+H* ⇌ H_2O* +*
(9) H_2O* ⇌ H_2O +*

Step 5 as RDS, step 8 as irreversible step, others as quasi-equilibrium; H*, CO*, C* as MASI.

$$v_{CH_4} = \frac{(k_5K_9K_2K_3K_4P_{CO_2}k_8)^{1/2}\left(K_1P_{H_2}\right)^{\frac{3}{2}}}{(2K_7P_{H_2O})^{1/2}\{1+(K_1P_{H_2})^{\frac{1}{2}}+\frac{K_9K_2K_3P_{CO_2}(K_1P_{H_2})^1}{P_{H_2O}}+\frac{(K_9K_2K_3K_4P_{CO_2}k_8)^{1/2}\left(K_1P_{H_2}\right)^{\frac{1}{2}}}{(2k_5K_7P_{H_2O})^{1/2}}\}^3} \quad \text{(C4)}$$

D: CO_2* →HCOO*→CO*→HCO*→ C* or CH_x*

(1) H_2 + 2* ⇌ 2H*
(2) CO_2 + H* ⇌ HCOO*
(3) HCOO* +* ⇌ CO*+OH*
(4) CO* + H* ⇌ HCO* + *
(5) HCO* + * ⇌ CH*+O*
(6) CH* + 3H* ⇌ CH_4* + 3*
(7) O*+H* ⇌ OH* +*
(8) OH*+H* ⇌ H_2O* +*

Step 5 as RDS, step 8 as irreversible step, others as quasi-equilibrium; CO*, HCO*, O* as MASI.

$$v_{CH_4} = \frac{(K_2K_3K_4k_8k_5P_{CO_2})^{\frac{1}{2}}(K_1P_{H_2})^{\frac{3}{4}}}{(2)^{1/2}\{1+(\frac{k_8K_3K_2P_{CO_2}}{2k_5K_4})^{\frac{1}{2}}\left(K_1P_{H_2}\right)^{\frac{3}{4}}+(\frac{K_2K_3K_4k_8P_{CO_2}}{2k_5})^{\frac{1}{2}}\left(K_1P_{H_2}\right)^{\frac{3}{4}}+(\frac{2k_5K_2K_3K_4P_{CO_2}}{k_8{K_7}^2})^{1/2}(K_1P_{H_2})^{\frac{-1}{4}}} \quad \text{(D1)}$$

(1) H_2 + 2* ⇌ 2H*
(2) CO_2 + H* ⇌ HCOO*
(3) HCOO* +* ⇌ CO*+OH*
(4) CO* + H* ⇌ HCO* + *
(5) HCO* + * ⇌ C*+OH*
(6) C* + 2H* ⇌ CH_2* + 2*
(7) CH_2*+2H* ⇌ CH_4* +2*
(8) OH*+H* ⇌ H_2O* +*

Step 6 as RDS, step 8 as irreversible step, others as quasi-equilibrium; H*, HCO*, OH* as MASI

$$v_{CH_4} = \frac{k_6(k_8)^{\frac{2}{3}}\left(K_3K_2P_{CO_2}\right)^{\frac{1}{3}}K_1P_{H_2}}{(2k_7)^{\frac{1}{3}}\{1+(K_2P_{H_2})^{\frac{1}{2}}+\frac{(k_8)^{1/3}(K_3K_2P_{CO_2})^{2/3}(K_1P_{H_2})^{\frac{1}{2}}}{(2k_7)^{1/3}}+(\frac{2k_7K_3K_2P_{CO_2}}{k_8})^{1/3}(K_1P_{H_2})^{1/2}\}^2} \quad \text{(D2)}$$

(1) H_2 + 2* ⇌ 2H*
(2) CO_2 + H* ⇌ HCOO*
(3) HCOO* +* ⇌ CO*+OH*
(4) CO* + H* ⇌ HCO* + *
(5) HCO* + H* ⇌ CH*+OH*
(6) CH* + 3H* ⇌ CH_4* + 3*
(7) OH*+H* ⇌ H_2O* +*

Step 5 as RDS, step 8 as irreversible step, others as quasi-equilibrium; H*, HCO*, OH* as MASI.

$$v_{CH_4} = \frac{k_5(k_7K_3K_2P_{CO_2})^{1/2}(K_1P_{H_2})^1}{(2k_5)^{\frac{1}{2}}\{1+(K_1P_{H_2})^{\frac{1}{2}}+(\frac{2k_5K_3K_2P_{CO_2}(K_1P_{H_2})^1}{k_7})^{\frac{1}{2}}+\frac{(k_7K_3K_2P_{CO_2})^{1/2}(K_1P_{H_2})^{1/2}}{(2k_5)^{\frac{1}{2}}}\}^2} \quad \text{(D3)}$$

(1) H_2 + 2* ⇌ 2H*
(2) CO_2 + H* ⇌ HCOO*
(3) HCOO* +* ⇌ CO*+OH*
(4) CO* + H* ⇌ HCO* + *
(5) HCO* + 2H* ⇌ CH_2*+OH*+*
(6) CH_2* + 2H* ⇌ CH_4* + 2*
(7) OH*+H* ⇌ H_2O* +*

Step 5 as RDS, step 8 as irreversible step, others as quasi-equilibrium; H*, HCO*, OH* as MASI

$$v_{CH_4} = \frac{(k_5k_7K_3K_2P_{CO_2})^{1/2}\ (K_1P_{H_2})^{5/4}}{(2)^{\frac{1}{2}}\{1+(K_1P_{H_2})^{\frac{1}{2}}+\frac{(k_7K_3K_2P_{CO_2})^{1/2}\ (K_1P_{H_2})^{1/4}}{(2k_5)^{\frac{1}{2}}}+(\frac{2k_5K_3K_2P_{CO_2}}{k_7})^{\frac{1}{2}}\left(K_1P_{H_2}\right)^{\frac{3}{4}}\}^3} \quad \text{(D4)}$$

(1) H_2 + 2* ⇌ 2H*
(2) CO_2 + H* ⇌ HCOO*
(3) HCOO* + H* ⇌ CO*+H_2O*
(4) CO* + H* ⇌ HCO* +*
(5) HCO* + * ⇌ C*+OH*
(6) C* + H* ⇌ CH*+*
(7) CH* + 3H* ⇌ CH_4* + 3*
(8) OH*+H* ⇌ H_2O* +*
(9) H_2O* ⇌ H_2O +*

Step 5 as RDS, others as quasi-equilibrium; H*, CO* as MASI

$$v_{CH_4} = \frac{k_5K_9K_4K_3(K_2P_{CO_2})(K_1P_{H_2})^{3/2}}{P_{H_2O}\{1+{K_1}^{0.5}{P_{H_2}}^{0.5}+\frac{K_3(K_2P_{CO_2})(K_1P_{H_2})}{P_{H_2O}}\}^2} \quad \text{(D5a)}$$

Step 6 as RDS, step 8 as irreversible step, others as quasi-equilibrium; H*, CO* and HCO* as MASI

$$v_{CH_4} = \frac{(k_6k_9K_5K_9K_4K_3K_2P_{CO_2})^{1/2}(K_1P_{H_2})^{7/4}}{(P_{H_2O})^{\frac{1}{2}}\{1+{K_1}^{0.5}{P_{H_2}}^{0.5}+\frac{K_3(K_2P_{CO_2})(K_1P_{H_2})}{P_{H_2O}}+\frac{K_4K_3(K_2P_{CO_2})(K_1P_{H_2})^{3/2}}{P_{H_2O}}\}^2} \quad \text{(D5b)}$$

(1) H_2 + 2* ⇌ 2H*
(2) CO_2 + H* ⇌ HCOO*
(3) HCOO* + H* ⇌ CO*+H_2O*
(4) CO* + H* ⇌ HCO*
(5) HCO* + H* ⇌ CH*+OH*
(6) CH* + H* ⇌ CH_2* + *
(7) CH_2* + 2H* ⇌ CH_4* + 2*
(8) OH*+H* ⇌ H_2O* +*
(9) H_2O* ⇌ H_2O +*

Step 5 as RDS, step 8 as irreversible step, others as quasi-equilibrium; H*, CO* and HCO* as MASI

$$v_{CH_4} = \frac{(k_6k_8K_9K_4K_3K_2P_{CO_2})^{\frac{1}{2}}(K_1P_{H_2})^2}{(P_{H_2O})^{\frac{1}{2}}\{1+{K_1}^{0.5}{P_{H_2}}^{0.5}+\frac{K_3K_9K_2P_{CO_2}K_1P_{H_2}}{P_{H_2O}}+\frac{K_9K_4K_3K_2P_{CO_2}(K_1P_{H_2})^{3/2}}{P_{H_2O}}\}^2} \quad \text{(D6)}$$

Step 5 as RDS, other steps quasi-equilibrium; H*, CO* and HCO* as MASI.

$$v_{CH_4} = \frac{k_5K_4K_3(K_2P_{CO_2})(K_1P_{H_2})^2}{P_{H_2O}\{1+{K_1}^{0.5}{P_{H_2}}^{0.5}+\frac{K_3(K_2P_{CO_2})(K_1P_{H_2})}{P_{H_2O}}+\frac{K_4K_3(K_2P_{CO_2})(K_1P_{H_2})^{3/2}}{P_{H_2O}}\}^2} \quad \text{(D7a)}$$

(1) H_2 + 2* ⇌ 2H*
(2) CO_2 + H* ⇌ HCOO*
(3) HCOO* + H* ⇌ CO*+H_2O*
(4) CO* + H* ⇌ HCO*
(5) HCO* + H* ⇌ C*+H_2O
(6) C* + H* ⇌ CH* + *
(7) CH* + 3H* ⇌ CH_4* + 3*
(8) H_2O* ⇌ H_2O +*

Step 6 as RDS, other steps quasi-equilibrium; H*, CO*, C* as MASI.

$$v_{CH_4} = \frac{k_6K_5K_4K_3(K_2P_{CO_2})(K_1P_{H_2})^{2.5}}{P_{H_2O}{}^2\{1 + K_1{}^{0.5}P_{H_2}{}^{0.5} + \frac{K_3(K_2P_{CO_2})(K_1P_{H_2})}{P_{H_2O}} + \frac{K_5K_4K_3(K_2P_{CO_2})(K_1P_{H_2})^2}{P_{H_2O}{}^2}\}^2} \quad \text{(D7b)}$$

(1) H_2 + 2* ⇌ 2H*
(2) CO_2 + H* ⇌ HCOO*
(3) HCOO* + H* ⇌ CO*+H_2O*
(4) CO* + H* ⇌ HCO*+*
(5) HCO* + 2H* ⇌ CH*+H_2O*+*
(6) CH* + H* ⇌ CH_2* + *
(7) CH_2* + 2H* ⇌ CH_4* + 2*
(8) H_2O* ⇌ H_2O +*

Step 5 as RDS, others as quasi-equilibrium; H*, CO* and HCO* as MASI

$$v_{CH_4} = \frac{k_5K_8K_4K_3K_2P_{CO_2}(K_1P_{H_2})^{2.5}}{P_{H_2O}\{1 + (K_1P_{H_2})^{\frac{1}{2}} + \frac{K_8K_4K_3K_2P_{CO_2}(K_1P_{H_2})^{1.5}}{P_{H_2O}} + \frac{K_8K_3K_2P_{CO_2}(K_1P_{H_2})^{1}}{P_{H_2O}}\}^3} \quad \text{(D8)}$$

E: CO_2* →HCOO*→CO*→H_2CO*→ CH_x*

Step 4 as RDS, step 8 as irreversible, others as quasi-equilibrium; H*, OH* and CO* as MASI

$$v_{\mathrm{CH_4}} = \frac{(k_4k_8K_3K_2P_{CO_2})^{1/2}(K_1P_{H_2})^{\frac{3}{2}}}{(2)^{1/2}\{1 + (K_1P_{\mathrm{H_2}})^{\frac{1}{2}} + \frac{(k_8K_3K_2P_{\mathrm{CO_2}}K_1P_{\mathrm{H_2}})^{1/2}}{(2k_4)^{1/2}} + (\frac{2k_4K_3K_2P_{\mathrm{CO_2}}}{k_8})^{1/2}\}^3} \quad \text{(E1a)}$$

(1) H_2 + 2* ⇌ 2H*
(2) CO_2 + H* ⇌ HCOO*
(3) HCOO* +* ⇌ CO*+OH*
(4) CO* + 2H* ⇌ H_2CO* + 2 *
(5) H_2CO* + * ⇌ C*+H_2O*
(6) C* + 2H* ⇌ CH_2* + 2*
(7) CH_2* + 2H* ⇌ CH_4* + 2*
(8) OH*+H* ⇌ H_2O* +*
(9) H_2O* ⇌ H_2O +*

Step 5 as RDS, step 8 as irreversible, others as quasi-equilibrium; H*, H_2CO*, OH* and CO* as MASI

$$v_{\mathrm{CH_4}} = \frac{(k_8K_4K_3K_2P_{\mathrm{CO_2}})^{1/2}K_1P_{\mathrm{H_2}}}{(2k_5)^{1/2}\{1 + (K_1P_{\mathrm{H_2}})^{\frac{1}{2}} + \frac{(k_8K_4K_3K_2P_{\mathrm{CO_2}})^{1/2}}{(2k_5)^{1/2}}K_1P_{\mathrm{H_2}} + (\frac{2k_5K_4K_3K_2P_{\mathrm{CO_2}}K_1P_{\mathrm{H_2}}}{k_8})^{1/2} + \frac{(k_8K_3K_2P_{\mathrm{CO_2}})^{1/2}}{(2k_5K_4)^{1/2}}\}^2} \quad \text{(E1b)}$$

Step 6 as RDS, step 8 as irreversible, others as quasi-equilibrium; H*, H_2CO*, OH* and CO* as MASI.

$$v_{\mathrm{CH_4}} = \frac{(k_8K_9K_5K_4K_3K_2P_{\mathrm{CO_2}})^{1/2}(K_1P_{\mathrm{H_2}})^{3/2}}{(2k_6P_{H_2O})^{\frac{1}{2}}\{1 + (K_1P_{H_2})^{\frac{1}{2}} + \frac{(K_4K_3K_2P_{CO_2}k_8P_{H_2O}K_1P_{H_2})^{1/2}}{(2k_6K_9K_5)^{1/2}} + (\frac{2k_6K_9K_5K_4K_3K_2P_{CO_2}}{k_8P_{H_2O}})^{\frac{1}{2}}(K_1P_{H_2})^{1} + \frac{(k_8P_{H_2O}K_3K_2P_{CO_2})^{1/2}}{(2k_6K_9K_5K_4K_1P_{H_2})^{1/2}}\}^3} \quad \text{(E1c)}$$

(1) H_2 + 2* ⇌ 2H*
(2) CO_2 + H* ⇌ HCOO*
(3) HCOO* +* ⇌ CO*+OH*
(4) CO* + 2H* ⇌ H_2CO* + 2 *
(5) H_2CO* + H* ⇌ CH_2*+OH*+*
(6) CH_2* + 2H* ⇌ CH_4* + 2*
(7) OH*+H* ⇌ H_2O* +*

Step 5 as RDS, step 7 as irreversible, others as quasi-equilibrium; H*, H_2CO*, OH* and CO* as MASI

$$v_{\mathrm{CH_4}} = \frac{\left(k_5K_4k_7K_3K_2P_{\mathrm{CO_2}}\right)^{\frac{1}{2}}(K_1P_{\mathrm{H_2}})^{1/4}}{(2)^{1/2}\{1 + (K_1P_{\mathrm{H_2}})^{\frac{1}{2}} + \frac{(K_4k_7K_3K_2P_{\mathrm{CO_2}})^{1/2}}{(2k_5)^{1/2}K_1P_{\mathrm{H_2}}} + (\frac{2k_5K_4K_3K_2P_{\mathrm{CO_2}}}{k_7})^{\frac{1}{2}}(K_1P_{\mathrm{H_2}})^{3/2} + \frac{(k_7K_3K_2P_{\mathrm{CO_2}})^{1/2}}{(2k_5K_4)^{1/2}K_1P_{\mathrm{H_2}}}\}^2} \quad \text{(E2)}$$

(1) H_2 + 2* ⇌ 2H*
(2) CO_2 + H* ⇌ HCOO*
(3) HCOO* +* ⇌ CO*+OH*
(4) CO* + 2H* ⇌ H_2CO* + 2 *
(5) H_2CO* + 2H* ⇌ CH_3*+OH*+*
(6) CH_3* + H* ⇌ CH_4* + *
(7) OH*+H* ⇌ H_2O* +*

Step 5 as RDS, step 7 as irreversible, others as quasi-equilibrium; H*, H_2CO*, OH* and CO* as MASI

$$v_{\mathrm{CH_4}} = \frac{\left(k_5K_4k_7K_3K_2P_{\mathrm{CO_2}}\right)^{\frac{1}{2}}(K_1P_{\mathrm{H_2}})^{1/2}}{(2)^{1/2}\{1 + (K_1P_{H_2})^{\frac{1}{2}} + \frac{(K_4k_7K_3K_2P_{CO_2})^{1/2}(K_1P_{H_2})^{1/2}}{(2k_5)^{1/2}} + (\frac{2k_5K_4K_3K_2P_{CO_2}}{k_7})^{\frac{1}{2}}(K_1P_{H_2})^{1} + \frac{(k_7K_3K_2P_{CO_2})^{1/2}}{(2k_5K_4)^{\frac{1}{2}}(K_1P_{H_2})^{1/2}}\}^3} \quad \text{(E3)}$$

(1) H_2 + 2* ⇌ 2H*
(2) CO_2 + * ⇌ CO_2*
(3) CO_2* + H* ⇌ HCOO* + *
(4) HCOO* +H* ⇌ CO* + H_2O*
(5) CO* + 2H* ⇌ H_2CO* + 2*
(6) H_2CO* + H* ⇌ CH* + H_2O*
(7) CH* + 3H* ⇌ CH_4*
(8) H_2O* ⇌ H_2O + *
(9) CO* ⇌ CO + *

Step 6 as RDS, others as quasi-equilibrium; H*, H_2CO* and CO* as MASI.

$$v_{CH_4} = \frac{k_6K_3K_4K_6K_7K_2P_{CO_2}(K_1P_{H_2})^{2.5}}{P_{H_2O}\{1 + (K_1P_{\mathrm{H_2}})^{\frac{1}{2}} + \frac{K_1K_3K_7K_2P_{CO_2}P_{H_2}}{P_{H_2O}} + \frac{K_4K_2K_3K_6P_{CO_2}K_1{}^2P_{H_2}^2}{P_{H_2O}}\}^2} \quad \text{(E4)}$$

Step 5 as RDS, others as quasi-equilibrium; H*, CO_2* and CO* as MASI.

$$v_{\mathrm{CH_4}} = \frac{k_5K_4\ K_3K_8(K_2P_{\mathrm{CO_2}})(K_1P_{\mathrm{H_2}})^2}{P_{\mathrm{H_2O}}\{1 + \frac{K_4\ K_3K_8(K_2P_{\mathrm{CO_2}})(K_1P_{\mathrm{H_2}})}{P_{\mathrm{H_2O}}} + K_2P_{\mathrm{CO_2}} + (K_1P_{\mathrm{H_2}})^{\frac{1}{2}}\}^3} \quad \text{(E5a)}$$

Step 6 as RDS, other steps as quasi-equilibrium; H*, H_2CO * and CO* as MASI.

(1) $H_2 + 2^* \rightleftharpoons 2H^*$
(2) $CO_2 + ^* \rightleftharpoons CO_2^*$
(3) $CO_2^* + H^* \rightleftharpoons HCOO^* + ^*$
(4) $HCOO^* + H^* \rightleftharpoons CO^* + H_2O^*$
(5) $CO^* + 2H^* \rightleftharpoons H_2CO^* + 2^*$
(6) $H_2CO^* + ^* \rightleftharpoons C^* + H_2O^*$
(7) $C^* + 2H^* \rightleftharpoons CH_2^*$
(8) $CH_2^* + 2H^* \rightleftharpoons CH_4^* + 2^*$
(9) $H_2O^* \rightleftharpoons H_2O + ^*$
(10) $CO^* \rightleftharpoons CO + ^*$

$$v_{CH_4} = \frac{k_6 K_9 K_4 K_3 (K_2 P_{CO_2})(K_1 P_{H_2})^2}{P_{H_2O}\{1 + {K_1}^{0.5} {P_{H_2}}^{0.5} + \frac{K_9 K_4 K_3 (K_2 P_{CO_2})(K_1 P_{H_2})}{P_{H_2O}} + \frac{K_9 K_4 K_3 (K_2 P_{CO_2})(K_1 P_{H_2})^2}{P_{H_2O}}\}^2} \quad \text{(E5b)}$$

Step 7 as RDS, other steps as quasi-equilibrium; H_2CO * and CO* as MASI.

$$v_{CH_4} = \frac{k_7 {K_9}^2 K_6 K_5 K_4 K_3 (K_2 P_{CO_2})(K_1 P_{H_2})^3}{{P_{H_2O}}^2\{1 + \frac{K_9 K_4 K_3 (K_2 P_{CO_2})(K_1 P_{H_2})}{P_{H_2O}} + \frac{K_5 K_9 K_4 K_3 (K_2 P_{CO_2})(K_1 P_{H_2})^2}{P_{H_2O}}\}^3} \quad \text{(E5c)}$$

Step 6 as RDS and other steps as quasi-equilibrium; H_2CO* and CO* as MASI.

$$v_{CH_4} = \frac{K_5 K_2 K_8 K_4 K_3 k_6 P_{CO_2}^1 {K_1}^3 P_{H_2}^3}{P_{H_2O}[1 + \frac{K_4\ K_3 K_8 (K_2 P_{CO_2})(K_1 P_{H_2})}{P_{H_2O}} + \frac{K_5 K_3 K_4 K_8 (K_2 P_{CO_2})({K_1}^2 {P_{H_2}}^2)}{P_{H_2O}}]^3} \quad \text{(E6a)}$$

Step 6 as RDS, step 4 and 9 as irreversible, others as quasi-equilibrium; H_2CO* and CO* as MASI.

(1) $H_2 + 2^* \rightleftharpoons 2H^*$
(2) $CO_2 + ^* \rightleftharpoons CO_2^*$
(3) $CO_2^* + H^* \rightleftharpoons HCOO^* + ^*$
(4) $HCOO^* + H^* \rightleftharpoons CO^* + H_2O^*$
(5) $CO^* + 2H^* \rightleftharpoons H_2CO^* + 2^*$
(6) $H_2CO^* + 2H^* \rightarrow CH_2^* + H_2O^* + ^*$
(7) $CH_2^* + 2H^* \rightarrow CH_4^* + 2^*$
(8) $H_2O^* \rightarrow H_2O + ^*$
(9) $CO^* \rightarrow CO + ^*$

$$v_{CH_4} = \frac{{K_1}^3 K_2 k_4 k_6 K_3 K_5 P_{CO_2} {P_{H_2}}^3}{P_{H_2O}\{1 + \frac{k_4 K_3 (K_2 P_{CO_2})(K_1 P_{H_2})^1}{k_9 + k_6 K_5 (K_1 P_{H_2})^2} + \frac{k_4 K_3 K_5 (K_2 P_{CO_2})(K_1 P_{H_2})^2}{k_9 + k_6 K_5 (K_1 P_{H_2})^2}\}^3} \quad \text{(E6b)}$$

Step 6 as RDS, others as quasi-equilibrium; H* and CO_2* as MASI.

$$v_{CH_4} = \frac{K_5 K_2 K_8 K_4 K_3 k_6 P_{CO_2}^1 {K_1}^3 P_{H_2}^3}{P_{H_2O}[1 + K_1^{0.5} P_{H_2}^{0.5} + K_2 P_{CO_2}]^3} \quad \text{(E6c)}$$

i.e. RDS: rate determining step; MASI: most abundant surface intermediates; total 40 expression.

Table S4 Goodness of non-linear curve fitting using parameters of Adj. R^2 in generalized rate equations, $v_{CH_4} = \frac{k[\mathrm{H_2}]^{m1}}{\{K_1[\mathrm{H_2}]^{m2}+K_2[\mathrm{H_2}]^{m3}+K_3[\mathrm{H_2}]^{m4}+K_5\}^n}$.

Rate equation in Table 3	(m_1; m_2; m_3; m_4; n)	0.5 W•cm^{-2}	1.0 W•cm^{-2}	1.5 W•cm^{-2}	Dark (330 ºC)	Dark (510 ºC)
E5c; E6a; E6b	(3, 1, 2, 0, 3)	0.996	0.993	0.997	0.997	0.992
E5a	(2, 0.5, 1, 0, 3)	0.971	0.868	-0.333	0.982	0.994
E5b	(2, 0.5, 1, 2, 2)	0.989	0.959	-0.598	0.981	0.994
E4; D7b	(2.5, 0.5, 1, 2, 2)	0.988	0.974	0.830	0.986	0.997
D6; D7a	(2, 0.5, 1, 1.5, 2)	0.970	0.890	-0.6	0.976	0.993
D8	(2.5, 0.5, 1, 1.5, 3)	0.992	0.972	0.720	0.988	0.997
E6c	(3, 0.5, 0, 0, 3)	0.663	0.727	0.839	0.800	0.918
E2	(0.25, 0.5, -1, 1.5, 2)	0.937	0.992	0.976	0.857	0.976
E3	(0.5, 0.5, 1, -0.5, 3)	0.945	0.890	0.890	0.540	0.984
D1	(0.75, 0.75, -0.25, 0, 2)	0.769	0.216	0.254	0.680	0.940
D5a	(1.5, 0.5, 1, 0, 2)	0.805	0.826	0.757	0.934	0.992
D5b	(7/4, 1, 1.5, 0, 2)	0.971	0.841	-0.6	0.970	0.898
D4	(1.25, 0.5, 0.25, 0.75, 3)	0.881	0.003	-0.600	0.922	0.848
D2; D3	(1, 0.5, 0, 0, 2)	0.771	-0.115	-0.143	0.803	-0.143
B6; C4; E1a; E1c	(1.5, 0.5, -0.5, 1, 3)	0.979	0.902	0.985	0.962	0.977
C1a	(0.5, 0.5, 0, 0, 2)	0.355	-0.142	-0.142	-0.142	-0.142
C1b	(5/6, 0.5, 0,0,2)	0.704	-0.143	-0.143	0.617	-0.143
C3	(1.25, 0.5, 1, 0.75, 0, 2)	0.888	0.125	-0.600	0.921	0.885
B1a; B4a	(0.75, 0.5, 0.25, 0, 2)	0.592	-0.333	-0.333	0.322	-0.333
B1b	(0.75,0.5,0.75,0,2)	0.593	0.683	-0.333	0.406	-0.333
B2; B4b	(1, 0.5, 0, 0, 2)	0.803	-0.115	-0.412	0.803	-0.412
B3	(1, 0.5, -0.5, 1, 3)	0.970	0.851	0.963	0.881	0.657
B4c; E1b	(1, 0.5, 1, 0, 2)	0.978	-0.187	0.600	0.923	-0.44
B5b	(1.25, 0.25, 0.5, 0.75, 2)	0.827	0.011	-0.6	0.892	0.838
A1a	(0.5, 0.5, -0.5, 0, 2)	0.551	0.653	0.636	0.542	0.989
A1b	(5/6, 0.5, 1/6, 0, 2)	0.654	-0.333	-0.333	0.553	-0.333
A1c; C2; B5b	(1, 0.5, 0, 0, 3)	0.806	-0.115	-0.143	0.829	-0.142

Note: The highlighted row shows the best fitting results regardless of illumination conditions.

References

1. K. D. Rasamani, J. J. Foley, B. Beidelman and Y. Sun, *Nano Research*, 2017, **10**, 1292-1301.
2. H. Yamada, C. Urata, H. Ujiie, Y. Yamauchi and K. Kuroda, *Nanoscale*, 2013, **5**, 6145-6153.
3. K. Yue, X. Zhang and F. Yu, *Journal of Thermal Science*, 2004, **13**, 255-258.
4. S. J. Norton and T. Vo-Dinh, *Journal of Applied Physics*, 2016, **119**, 083105.
5. H. H. Pennes, *Journal of applied physiology*, 1948, **1**, 93-122.
6. M. Kind, H. Martin, P. Stephan, W. Roetzel, B. Spang, H. Müller-Steinhagen, X. Luo, M. Kleiber, R. Joh and W. Wagner, *Journal*, 2010.
7. L. A. Bromley and C. R. Wilke, *Industrial & Engineering Chemistry*, 1951, **43**, 1641-1648.
8. J. P. Blitz, *Modern Techniques in Applied Molecular Spectroscopy*, 1998, **14**, 185.
9. P. B. Weisz and C. D. Prater, in *Advances in Catalysis*, eds. W. G. Frankenburg, V. I. Komarewsky and E. K. Rideal, Academic Press, 1954, vol. 6, pp. 143-196.
10. D. E. Mears, *Industrial & Engineering Chemistry Process Design and Development*, 1971, **10**, 541-547.
11. E. N. Fuller, P. D. Schettler and J. C. Giddings, *Industrial & Engineering Chemistry*, 1966, **58**, 18-27.
12. N. Wakao and J. M. Smith, *Chemical Engineering Science*, 1962, **17**, 825-834.
13. N. Wakao and T. Funazkri, *Chemical Engineering Science*, 1978, **33**, 1375-1384.
14. W. E. Ranz and W. R. Marshall, *Chem. eng. prog*, 1952, **48**, 141-146.
15. L. C. Young and B. A. Finlayson, *Industrial & Engineering Chemistry Fundamentals*, 1973, **12**, 412-422.
16. C. F. Chu and K. M. Ng, *AIChE Journal*, 1989, **35**, 148-158.
17. R. H. Perry, D. W. Green and J. O. Maloney, *Seventh, International edition*, 1997, 23-23.
18. K. K. Bando, K. Sayama, H. Kusama, K. Okabe and H. Arakawa, *Applied Catalysis A: General*, 1997, **165**, 391-409.
19. K. Zhao, L. Wang, E. Moioli, M. Calizzi and A. Züttel, *The Journal of Physical Chemistry C*, 2019, **123**, 8785-8792.
20. F. Solymosi and M. Lancz, *Journal of the Chemical Society, Faraday Transactions 1: Physical Chemistry in Condensed Phases*, 1986, **82**, 883-897.
21. F. Solymosi, A. Erdöhelyi and T. Bánsági, *Journal of the Chemical Society, Faraday Transactions 1: Physical Chemistry in Condensed Phases*, 1981, **77**, 2645-2657.
22. J. T. Yates Jr, T. M. Duncan, S. D. Worley and R. W. Vaughan, *The Journal of Chemical Physics*, 1979, **70**, 1219-1224.
23. C. D. Zeinalipour-Yazdi, A. L. Cooksy and A. M. Efstathiou, *The Journal of Physical Chemistry C*, 2007, **111**, 13872-13878.
24. G. J. Millar, C. H. Rochester and K. C. Waugh, *Journal of Catalysis*, 1995, **155**, 52-58.
25. J. J. Corral-Pérez, A. Bansode, C. S. Praveen, A. Kokalj, H. Reymond, A. Comas-Vives, J. VandeVondele, C. Copéret, P. R. von Rohr and A. Urakawa, *Journal of the American Chemical Society*, 2018, **140**, 13884-13891.
26. D. B. Clarke and A. T. Bell, *Journal of Catalysis*, 1995, **154**, 314-328.
27. J. Raskó, T. Kecskés and J. Kiss, *Journal of Catalysis*, 2004, **226**, 183-191.

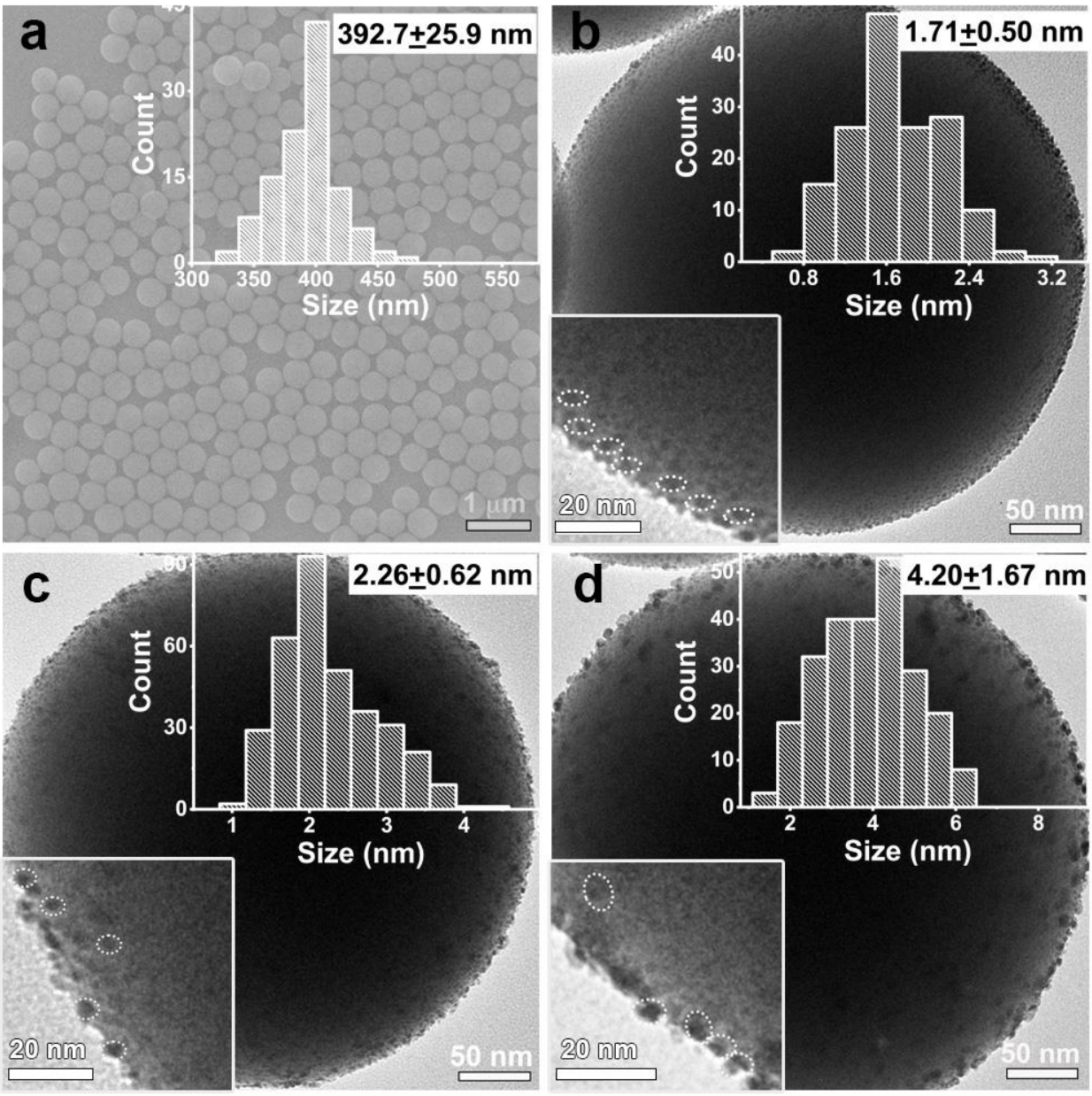

Figure S1. Electron microscopy characterization of silica nanospheres (SiO_x NSs) and Rh nanoparticles (NPs) on the SiO_x NSs. (a) Scanning electron microscopy (SEM) image and (inset) statistic histogram of size distribution of SiO_x NSs. (b, c, d) Transmission electron microscopy (TEM) images of Rh-NP/SiO_x-SP composite particles and (top right insets) statistic histograms of size distribution of Rh NPs with different average sizes b) 1.71 nm, c) 2.26 nm, and d) 4.20 nm. (Bottom left insets) TEM images with higher magnifications clearly showing the individual Rh NPs highlighted with dashed ellipses, which were used to determine the size of Rh NPs as shown in the statistic histograms shown in the top right insets.

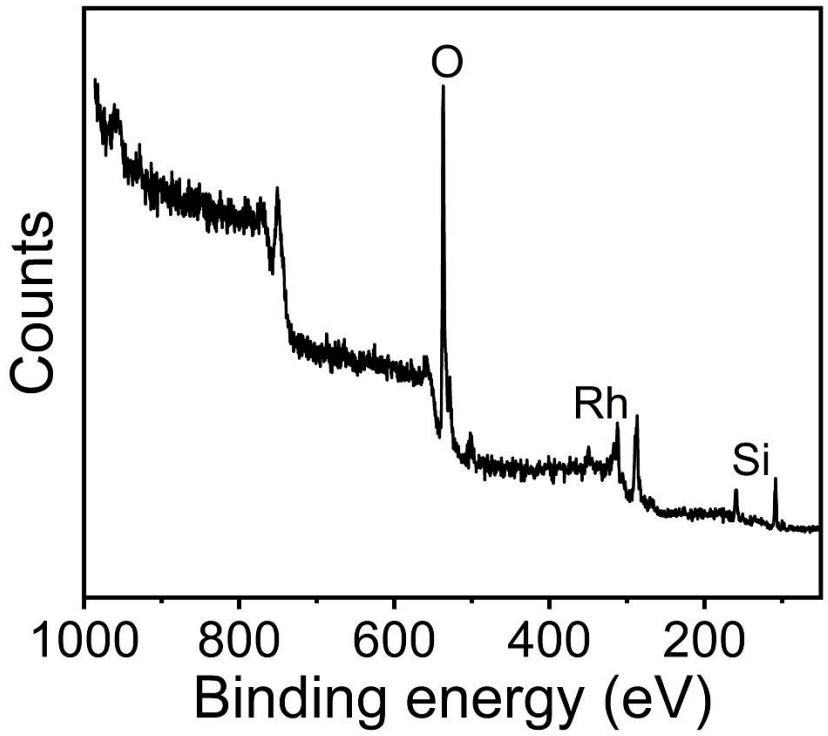

Figure S2. X-ray photoelectron spectroscopy (XPS) of Rh-NP/SiO_x-NS composite catalyst with Rh NPs of 2.26 nm in size. The sample was the same as that shown in Figure S1c.

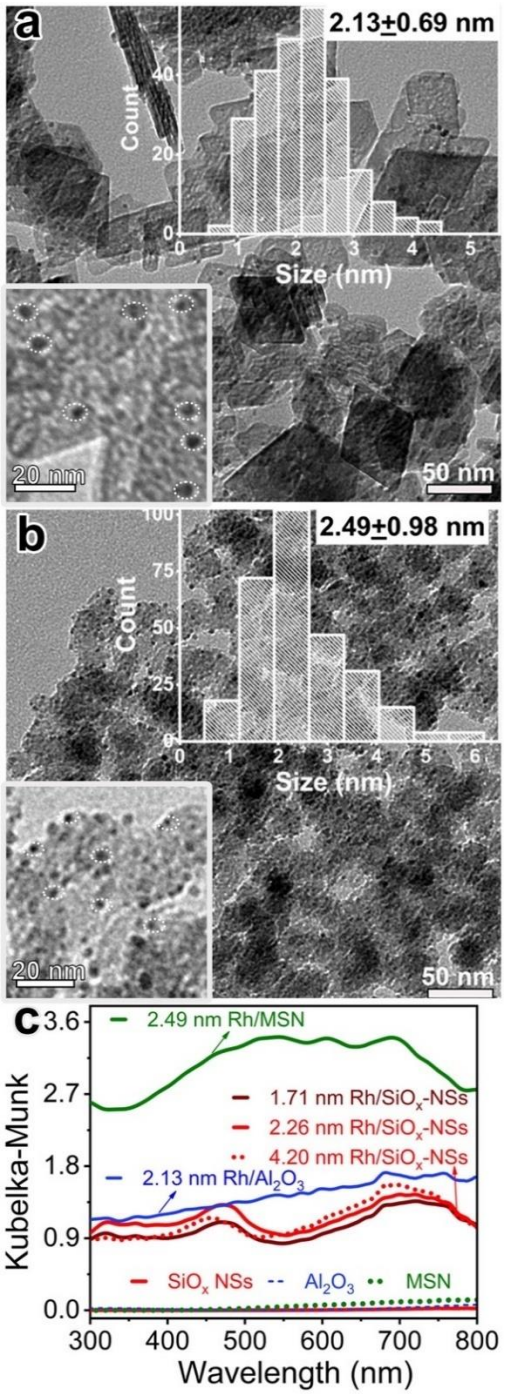

Figure S3. (a) TEM image of Rh/Al_2O_3 composite particles and (top right inset) statistic histogram of size distribution of the Rh NPs. (b) TEM image of Rh/MSN composite particles and (top right inset) statistic histogram of size distribution of the Rh NPs. (Bottom left insets in a, b) TEM images with higher magnifications clearly showing the individual Rh NPs highlighted with dashed ellipses, which were used to determine the size of Rh NPs as shown in the statistic histograms shown in the top right insets. (c) UV-vis diffuse reflectance spectra (DRS) of different powder samples: SiO_x NSs, Al_2O_3 nanoparticles, mesoporous silica nanoparticles (MSN), and Rh nanoparticles loaded on these oxide nanoparticles.

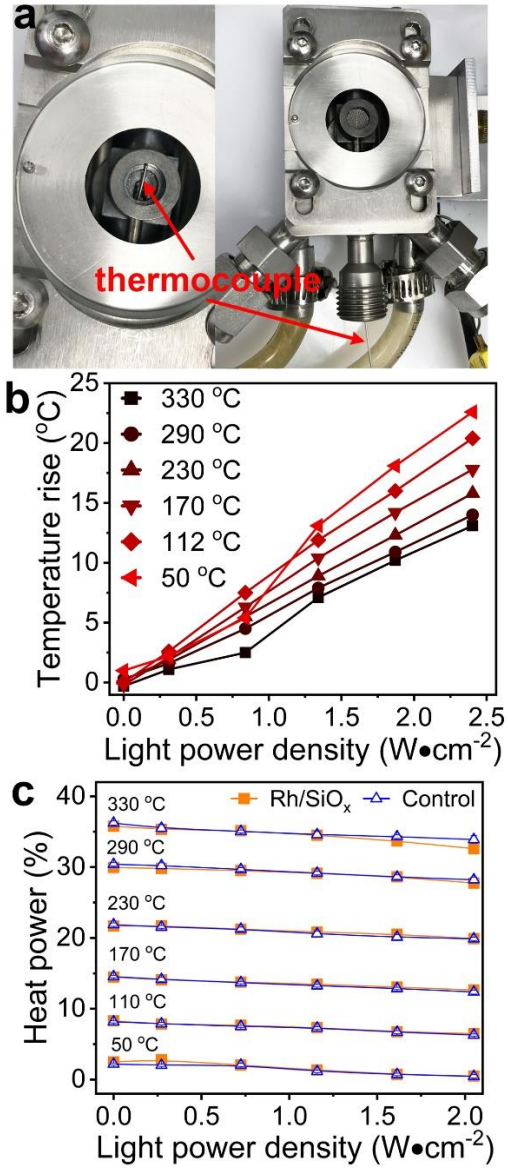

Figure S4. Evaluation of temperature change of the catalyst under photoillumination. (a) Digital photographs of the reactor highlighting the location of thermocouple wire (with a diameter of 0.3 mm) that was above the platinum mesh support and embedded in the catalyst powder. This thermocouple was added to directly measure the actual temperature of the catalyst powder. The built-in thermocouple calibrated for measuring and controlling the reactor chamber temperature is not shown in the photographs. (b) Temperature changes of the Rh-NP/SiO_x-NS catalysts under photoillumination of different light power densities when the reactor chamber temperature was set at different values. The temperature rise induced by the photothermal effect of the Rh NPs was measured by subtracting the temperature recorded from the SiO_x NS powder from the temperature recorded from the Rh-NP/SiO_x-NS powder while the reactant gases continuously flew through the reactor. (c) The variation of input heating power under photoillumination. The catalyst loaded to the reactor was 7.2 mg in mass, and the size of Rh NPs was 2.26 nm. The inlet gas included 35 $mL \cdot h^{-1}$ CO_2, 440 $mL \cdot h^{-1}$ H_2, and 85 $mL \cdot h^{-1}$ Ar.

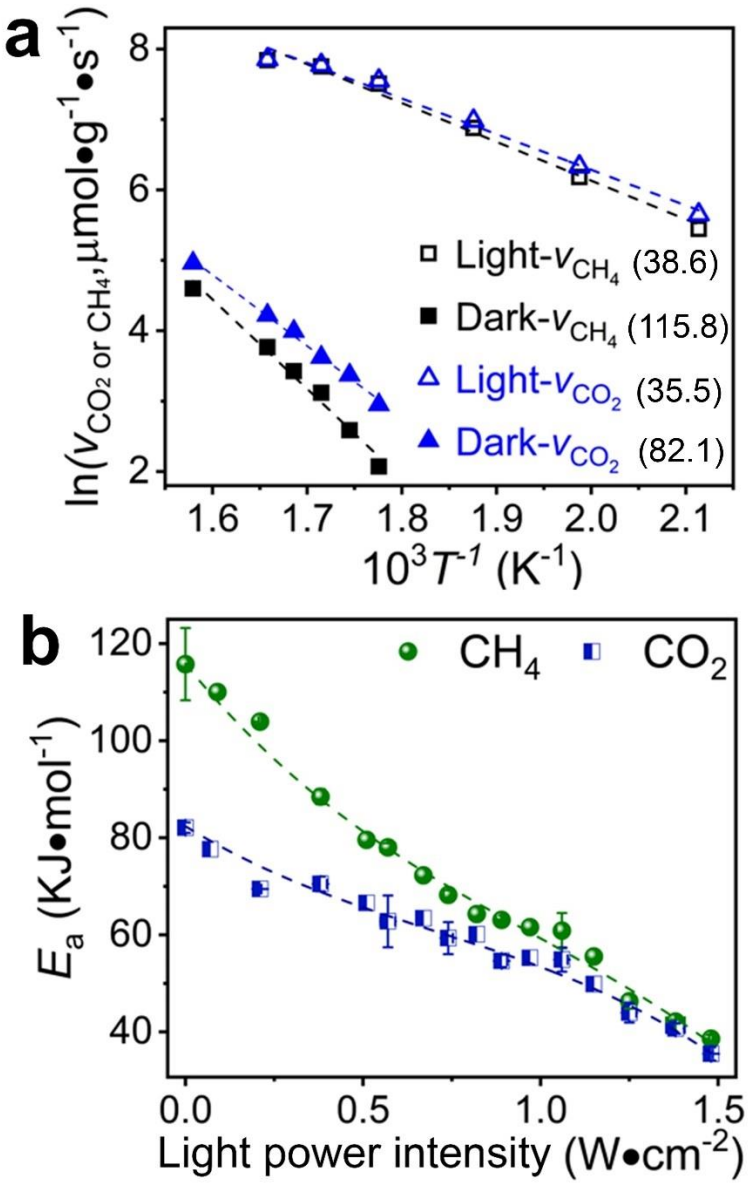

Figure S5. Apparent activation energy for CO_2 consumption and CH_4 production. (a) CO_2 consumption rate and CH_4 production rate in the natural logarithmic scale as a function of the reciprocal scale of thermodynamic temperature in the dark (black symbols) and under illumination of a light power intensity of 1.5 W·cm^{-2} (blue symbols). The values in the parentheses are the corresponding activation energies with the unit of kJ·mol^{-1} that derived from the slope of the linear fitting. (b) Dependence of CO_2 consumption activation energy (blue squares) and CH_4 production activation energy (green circles) on the light power intensity. The catalyst and reaction gas were the same as those in Figure S4.

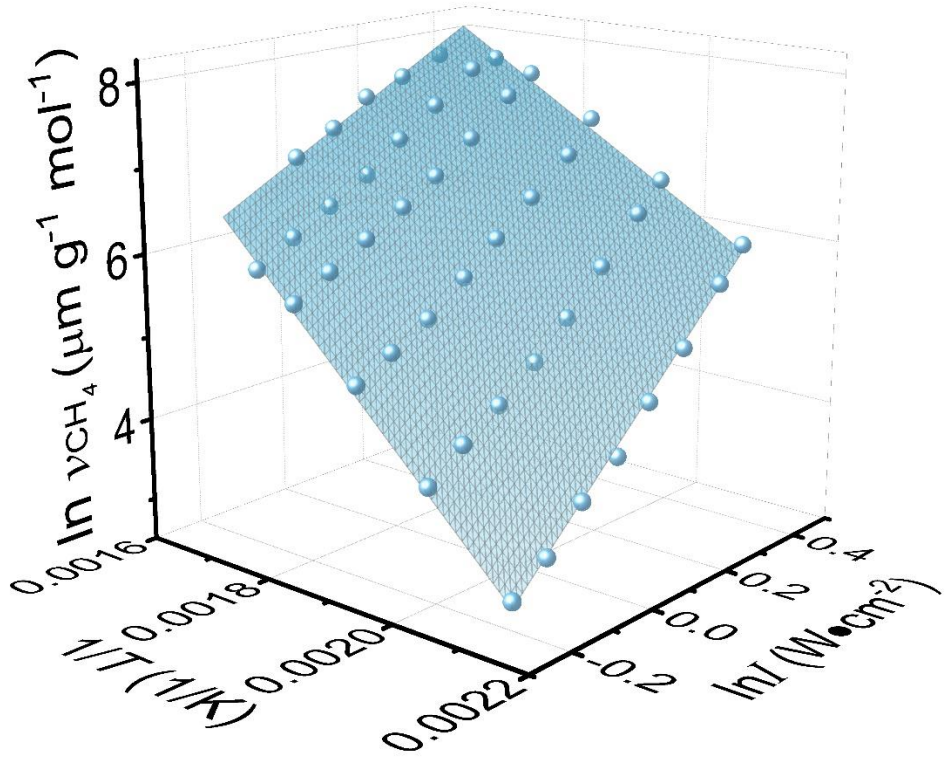

Figure S6. Non-linear surface fitting of the CH_4 production rate (v_{CH_4}) in the natural logarithmic scale as a function of the reciprocal of thermodynamic temperature (T) and the natural logarithm of the light power intensity (I) according to the equation $\ln v_{CH_4} = a + b \times T^{-1} + c \times \ln I + d \times T^{-1} \times \ln I$, in which a, b, and c are fitting constants.

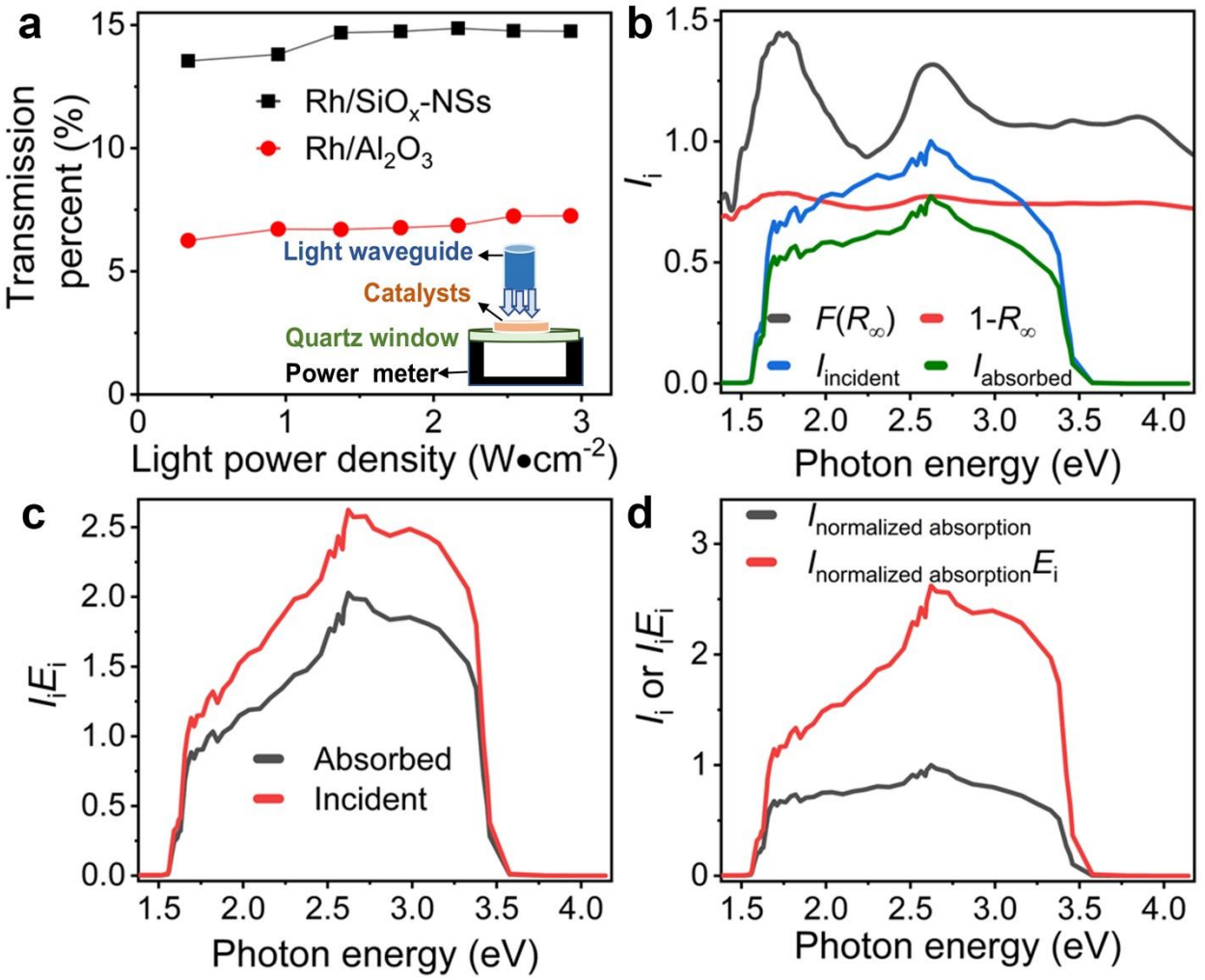

Figure S7. Estimation of the net optical absorption in the supported Rh NPs. (a) The percentage of light transmitted through the catalyst bed (e.g., Rh-NP/SiO_x-NS and Rh/Al_2O_3). The inset sketch shows the setup for measurements. (b) Kubelka-Munk intensity $F(R_\infty)$ (black curve), percentage of absorbed light ($1–R_\infty$) (red curve), intensity of incident light (blue curve), and calculated absorbed light intensity (green curve) as a function of photon energy. (c) Multiplication product of the incident light spectrum (red curve) or the absorbed light spectrum (black curve) and photon energy. (d) Multiplication product (red curve) of the normalized absorbed light spectrum (black curve) and photon energy. The results in (b-d) were measured from the Rh-NP/SiO_x-NS composite powder with 2.26-nm Rh NPs.

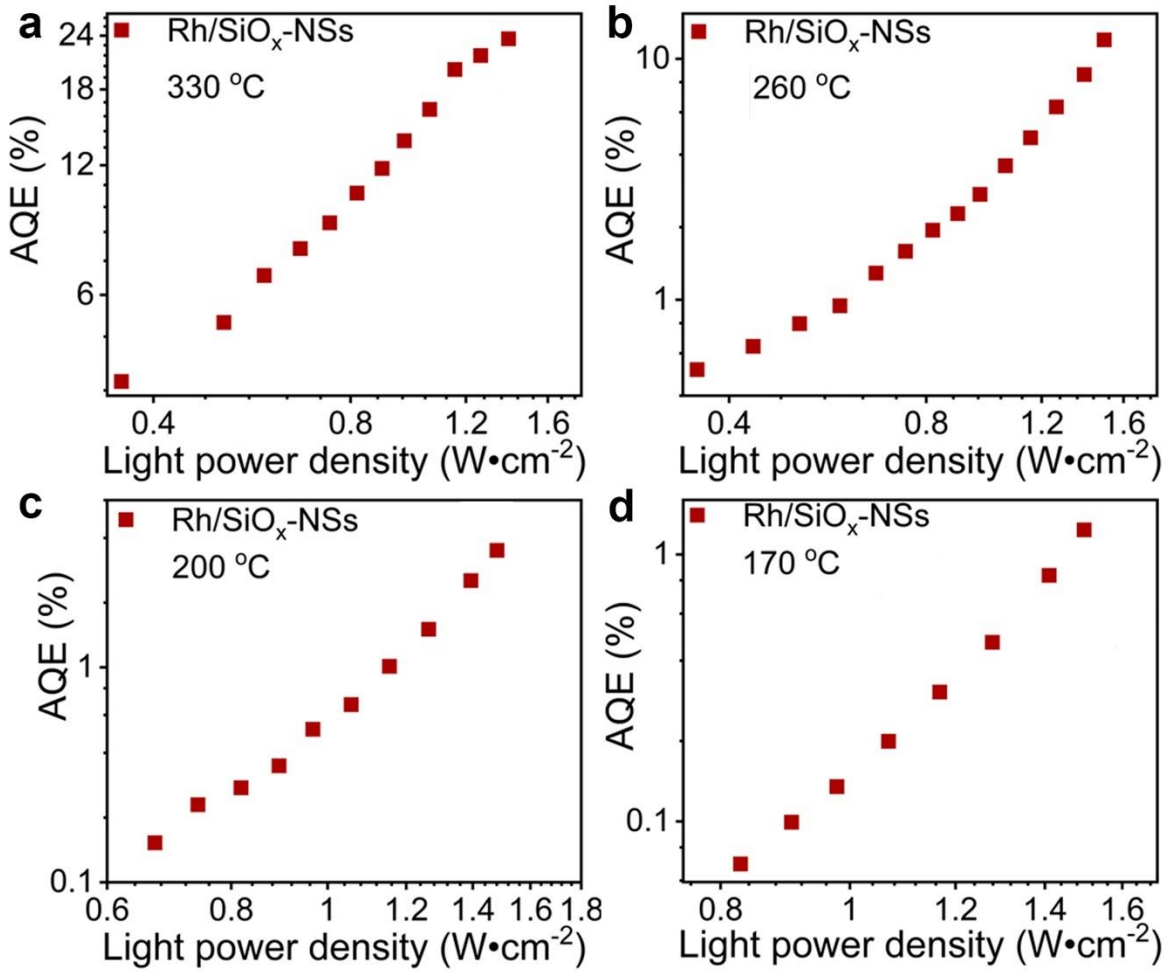

Figure S8. Apparent quantum efficiency (AQE) of CH_4 production as a function of light power intensity at different temperatures (a) 330 °C, (b) 260 °C, (c) 200 °C, and (d) 170 °C. The catalyst and reaction gas were the same as those in Figure S4.

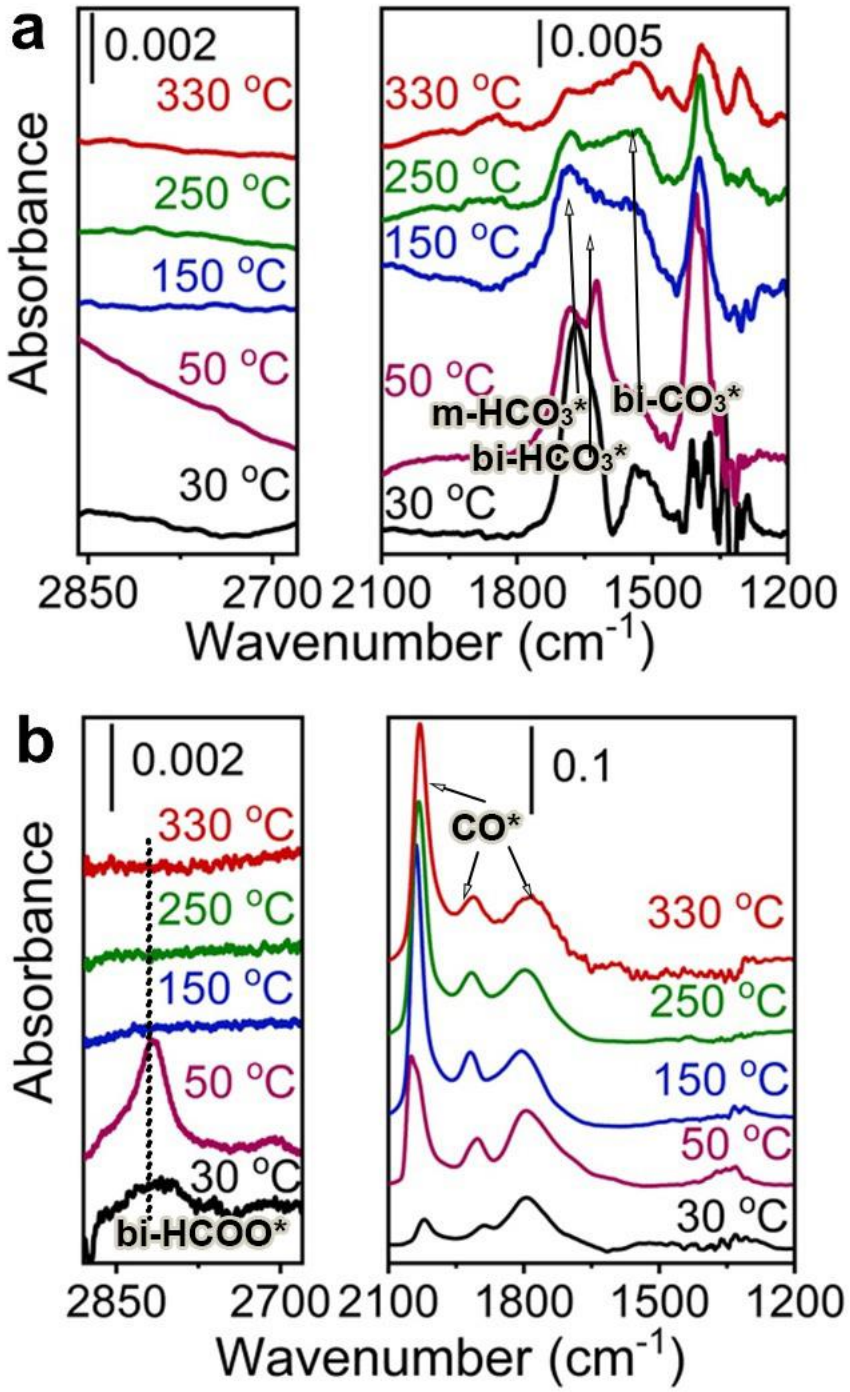

Figure S9. DRIFT spectra collected from Rh-NP/SiO_x-NS catalyst with Rh NPs of 2.26 nm in size. (a) Stabilized CO_2 adsorption on clean Rh surface at different temperatures in the gas flow containing 35 mL·h^{-1} CO_2 and 965 mL·h^{-1} Ar. Before performing measurement, the catalyst was reduced in a forming gas at 330 ºC followed by flowing Ar for 6 hours to remove the adsorbed hydrogen. (b) Steady-state adsorbates during CO_2 hydrogenation at different temperatures in the gas flow containing 35 mL·h^{-1} CO_2, 35 mL·h^{-1} H_2, and 960 mL·h^{-1} Ar.

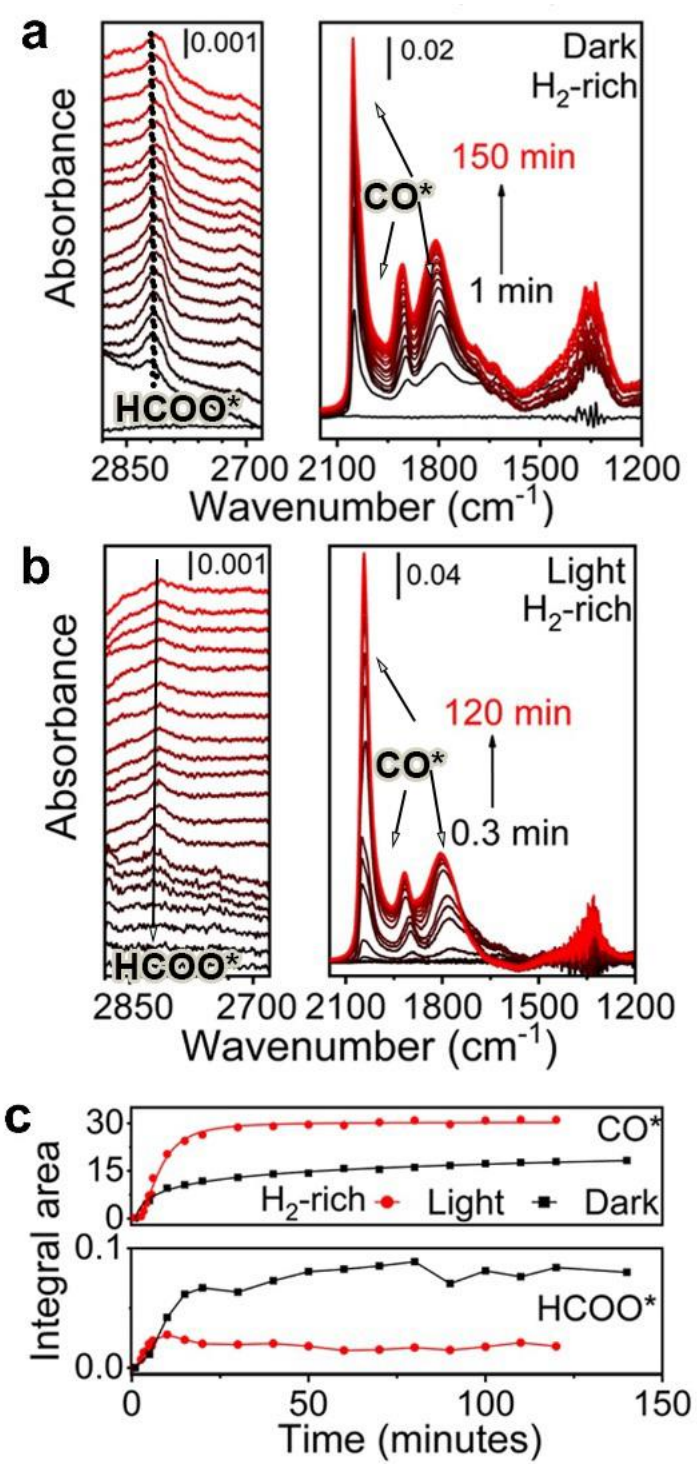

Figure S10. Time-dependent DRIFT spectra of the adsorbate species during CO_2 hydrogenation at 50 °C in a H_2-rich condition (35 mL·h^{-1} CO_2 + 350 mL·h^{-1} H_2 + 615 mL·h^{-1} Ar). (a) Spectra collected in the dark. (b) Spectra collected under photoillumination of a light power intensity of 1.5 W·cm^{-2}. (c) Integrated DRIFT peak area for all types of CO* (top panel) and bi-HCOO* (bottom panel) as a function of time. The catalyst was the same as that in Figure S4.

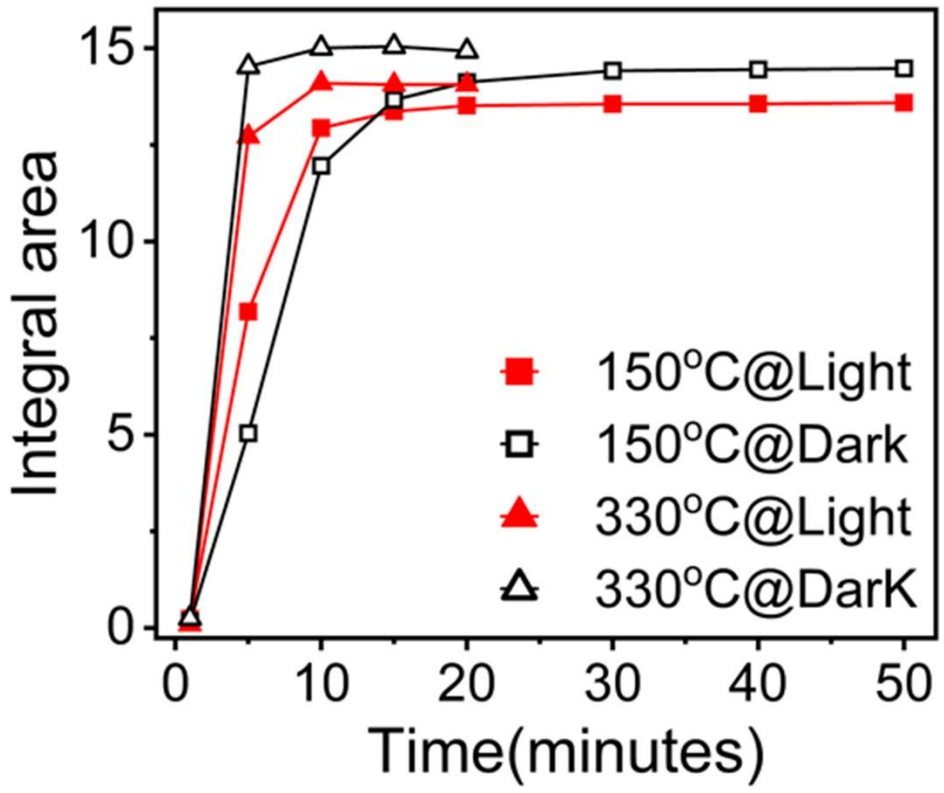

Figure S11. Time-dependent DRIFT peak area for all types of CO* during CO_2 hydrogenation in a H_2-lean condition (35 mL·h^{-1} CO_2 + 35 mL·h^{-1} H_2 + 960 mL·h^{-1} Ar) at 150 °C (square symbols) and 330 °C (triangle symbols). The catalyst was the same as that in Figure S4.

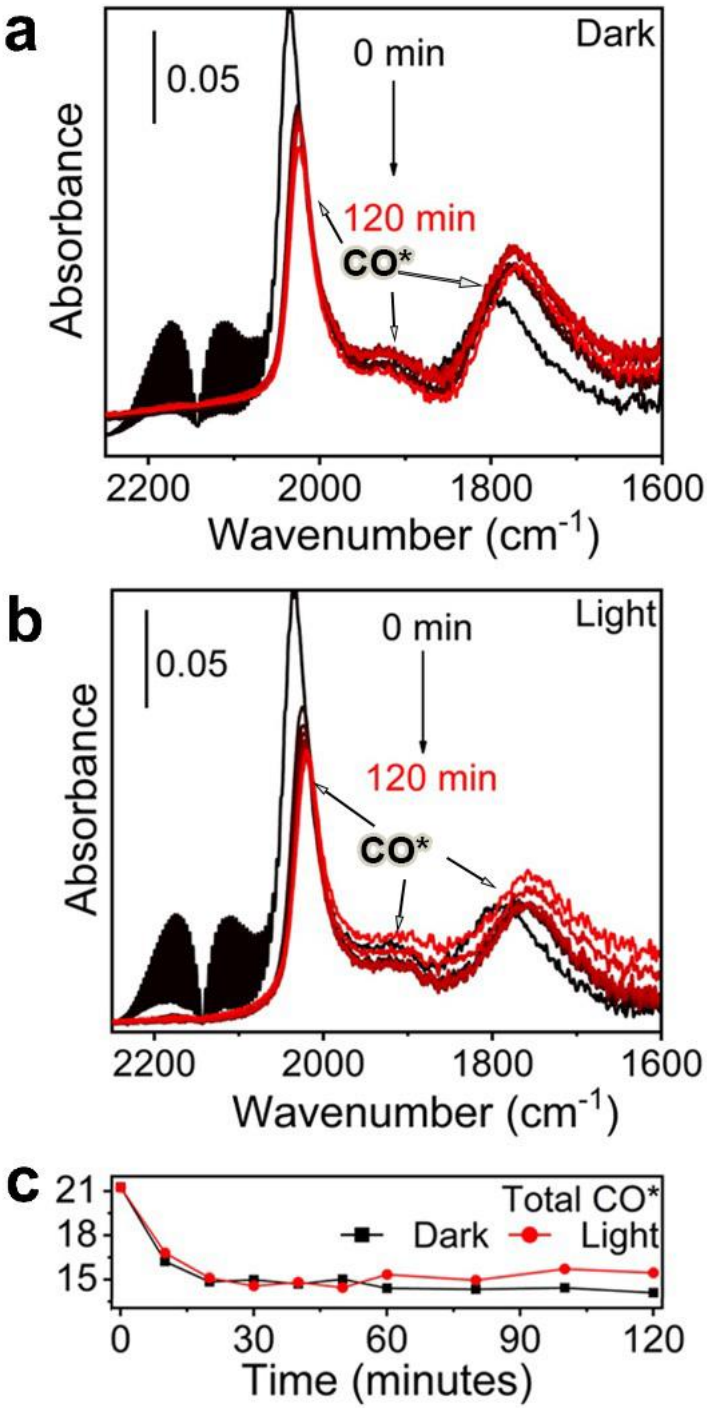

Figure S12. Time-dependent DRIFT spectra of CO* desorption in a gas flow of 1000 mL·h^{-1} Ar at 330 °C. Adsorption of CO* was achieved by flowing a gas mixture of 35 mL·h^{-1} CO and 965 mL·h^{-1} Ar at 330 °C for 50 minutes. (a) CO* desorption spectra in the dark. (b) CO* desorption spectra under photoillumination of a light power intensity of 1.5 W·cm^{-2}. (c) Integrated peak areas of all types of CO* as a function of desorption time. The catalyst was the same as that in Figure S4.

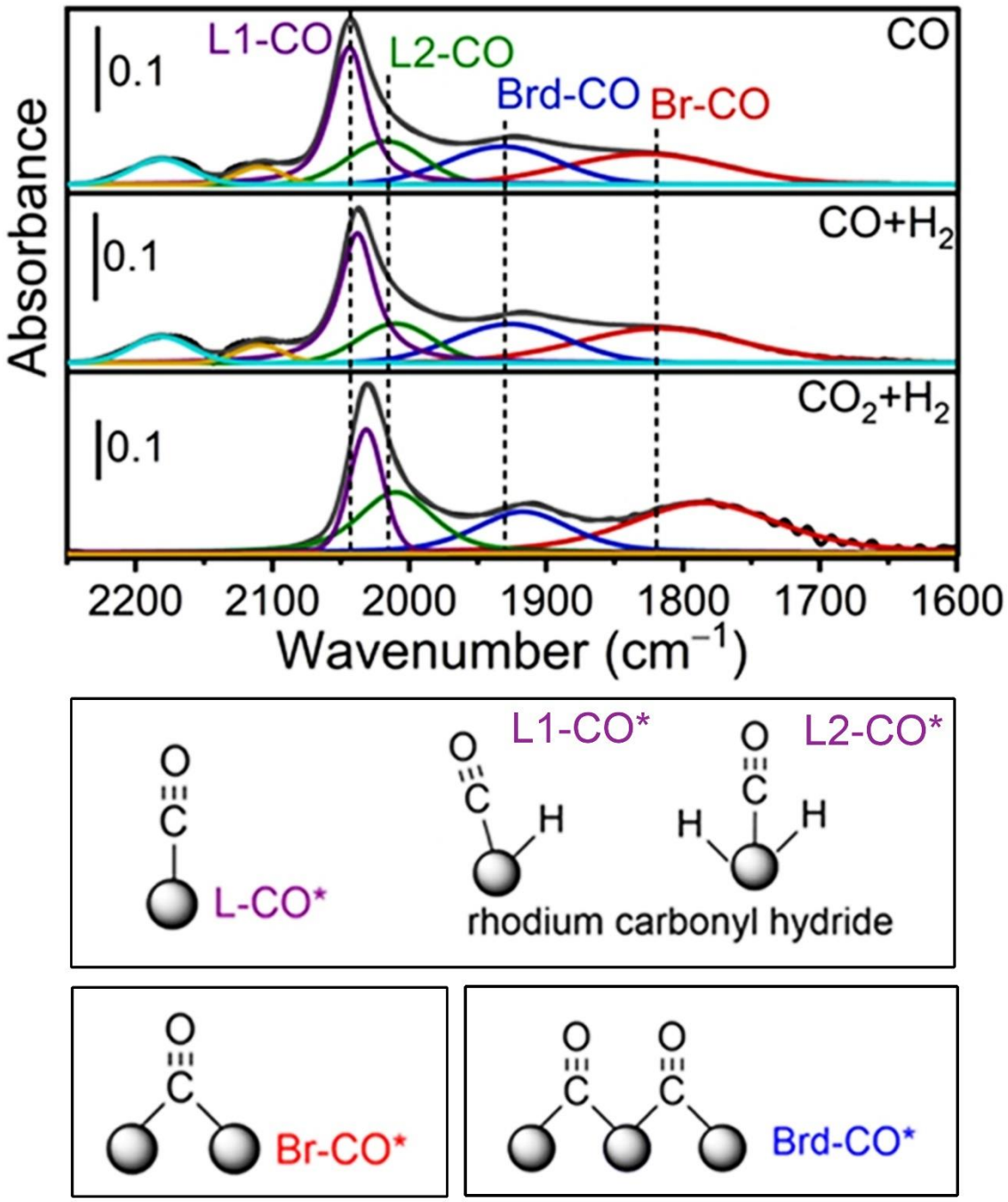

Figure S13. DRIFT spectra showing adsorption configurations of CO* on Rh-NP/SiO_x-NS catalyst at 330 ºC in different atmospheres: (top) 35 mL·h^{-1} CO + 965 mL·h^{-1} Ar, (middle) 35 mL·h^{-1} CO + 35 mL·h^{-1} H_2 + 930 mL·h^{-1} Ar, (bottom) 35 mL·h^{-1} CO_2 + 35 mL·h^{-1} H_2 + 930 mL·h^{-1} Ar. The catalyst was the same as that in Figure S4.

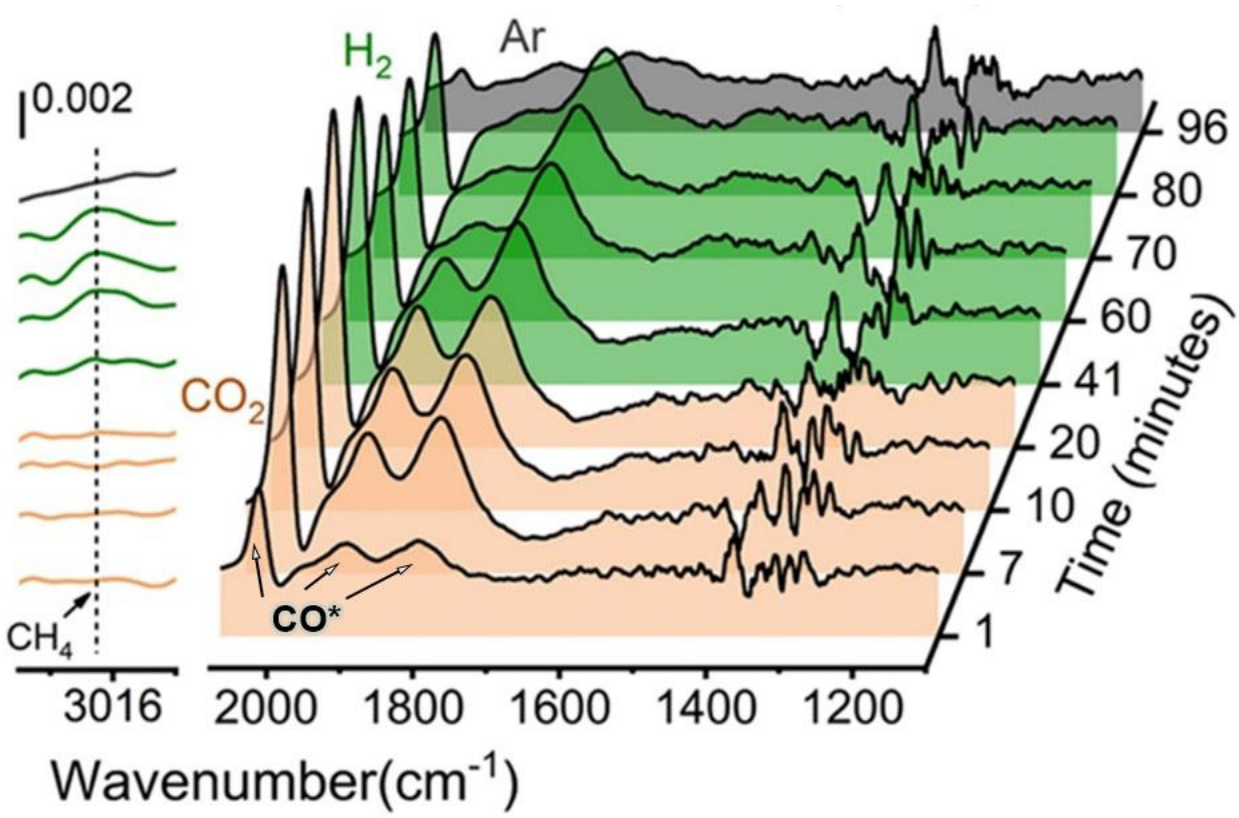

Figure S14. DRIFT spectra collected from the Rh-NP/SiO_x-NS catalyst at 330 ºC in the dark after the catalyst was reduced in the forming gas and blown by Ar for 30 minutes. The gas flow started with 35 mL·h^{-1} CO_2 + 965 mL·h^{-1} Ar for CO_2 (1-20 min), followed by 35 mL·h^{-1} H_2 + 965 mL·h^{-1} Ar (20-80 min) and then 1000 mL·h^{-1} Ar (80-96 min). The catalyst was the same as that in Figure S4.

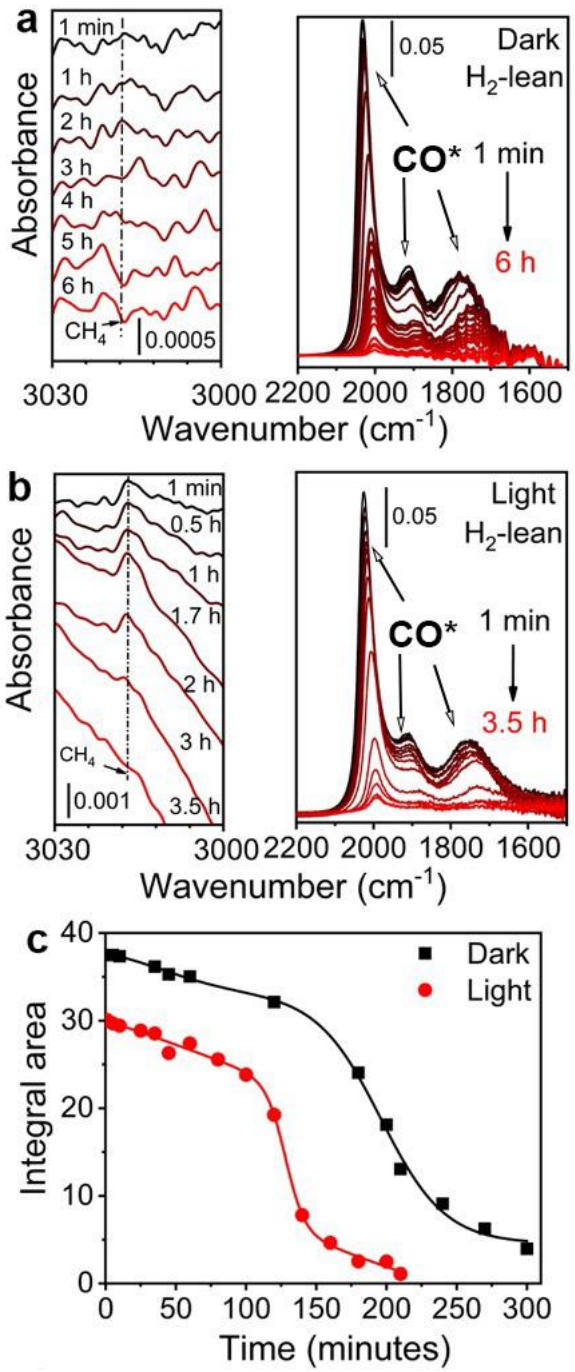

Figure S15. DRIFT spectra recorded after CO_2 hydrogenation reaction at 330 °C while exposing the catalyst to a H_2-lean condition with a gas flow containing 35 mL·h^{-1} H_2 and 965 mL·h^{-1} Ar. The pre-hydrogenation reaction was performed using the conditions same as Figure 1, leaving the steady-state coverage of CO* to allow studying the deoxygenation of CO*. (a) Time-dependent DRIFT spectra collected in the dark. (b) Time-dependent DRIFT spectra collected under photoillumination of a light power intensity of 1.5 W·cm^{-2}. (c) Time-dependent area of CO* derived from the spectra shown in (a, b), showing the faster deoxygenation kinetics under photoillumination.

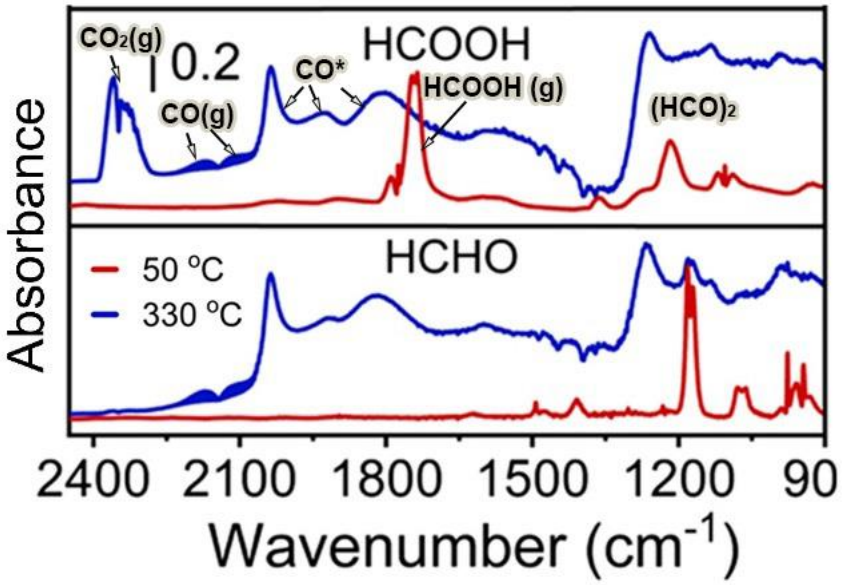

Figure S16. DRIFT spectra of (top) formic acid and (bottom) formaldehyde adsorbed on the Rh-NP/SiO_x-NS catalyst at 50 °C and 330 °C. The adsorption was achieved by flowing 1000 mL·h^{-1} Ar through a reservoir of liquid formic acid or trioxane (cyclic trimer of formaldehyde). The spectra at 330 °C are similar to those of CO_2 hydrogenation in the range of 1700-2050 cm^{-1}, which corresponds to CO*.

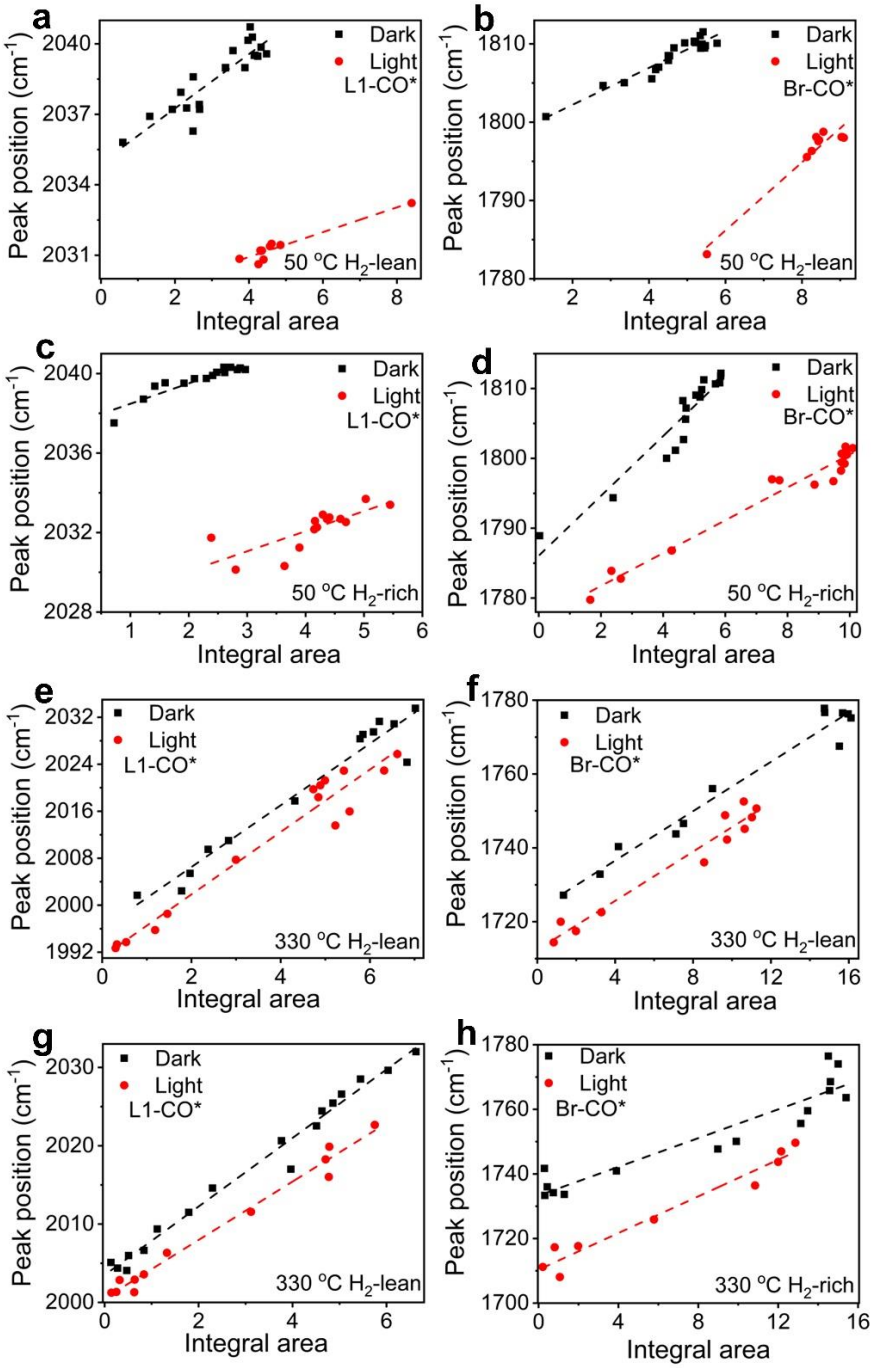

Figure S17. DRIFT spectral peak positions of L1-CO* and Br-CO* as a function of the corresponding peak areas at different temperatures (50 °C and 330 °C) and different H_2 concentrations. (a, b) data points derived from Figure 4a and 4b. (c, d) data points derived from Figure S10a and S10b. (e, f) data points derived from Figure S15a and S15b. (g, h) data points derived from Figure 4d and 4e. The peak positions under photoillumination are always at lower wavenumbers that those in the dark, indicating that C-O bond is weakened under photoillumination.

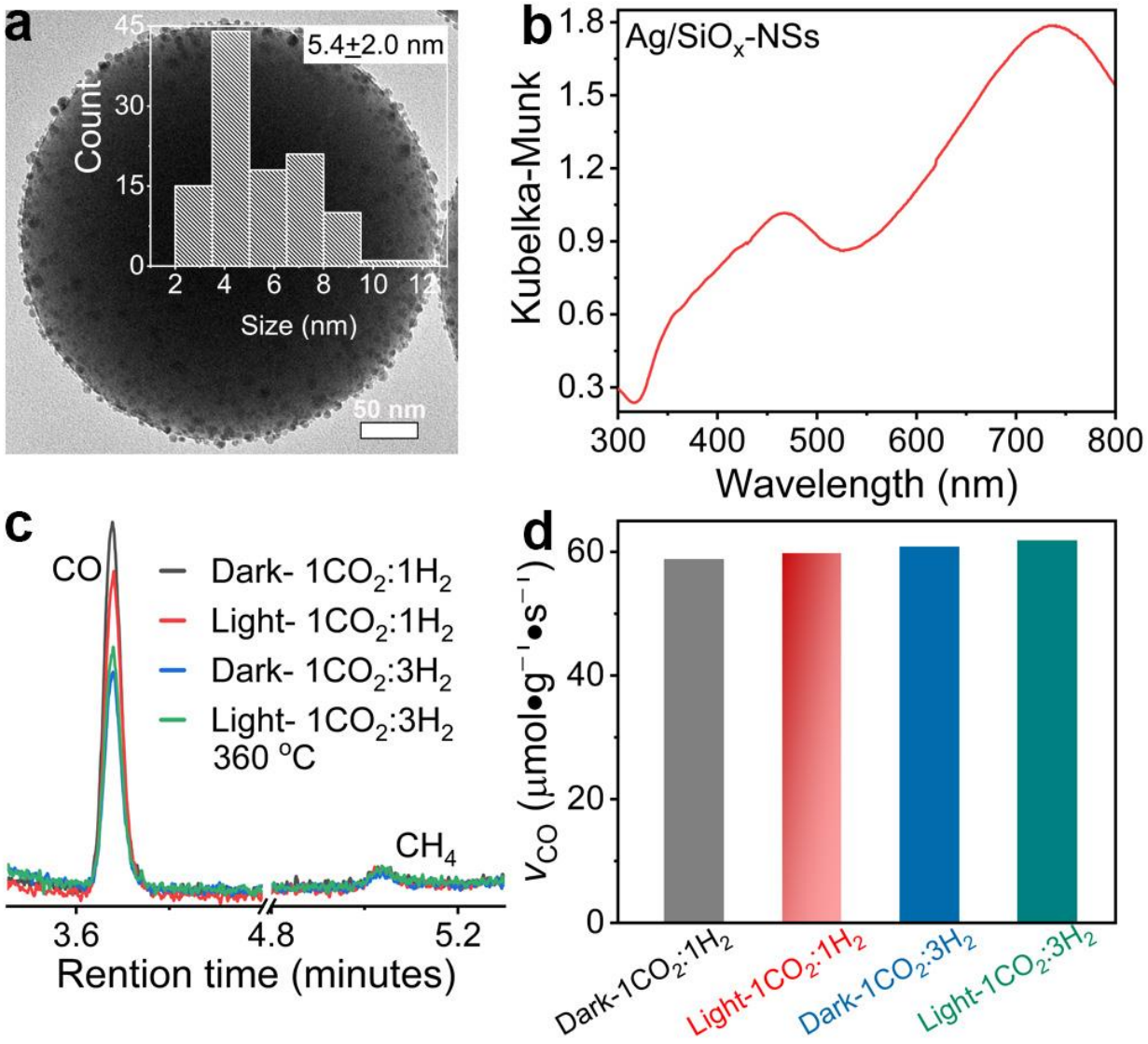

Figure S18. Characterization of Ag-NP/SiO_x-NS catalyst and CO_2 hydrogenation. (A) TEM image of a typical Ag-NP/SiO_x-NS composite particle. The inset shows the statistic histogram of size distribution of the Ag NPs. (B) DRS spectrum of the composite particle powder. (c) GC graphs of the CO_2 hydrogenation product using the Ag-NP/SiO_x-NS composite catalyst at 360 °C under different conditions. (d) Corresponding CO production rate calculated from (c). The total gas flow rate was 560 mL·h^{-1}. For $1CO_2$:$1H_2$ reaction, the gas flow contained 80 mL·h^{-1} Ar, 240 mL·h^{-1} CO_2, and 240 mL·h^{-1} H_2. For $1CO_2$:$1H_2$ reaction, the gas flow contained 80 mL·h^{-1} Ar, 120 mL·h^{-1} CO_2, and 360 mL·h^{-1} H_2.

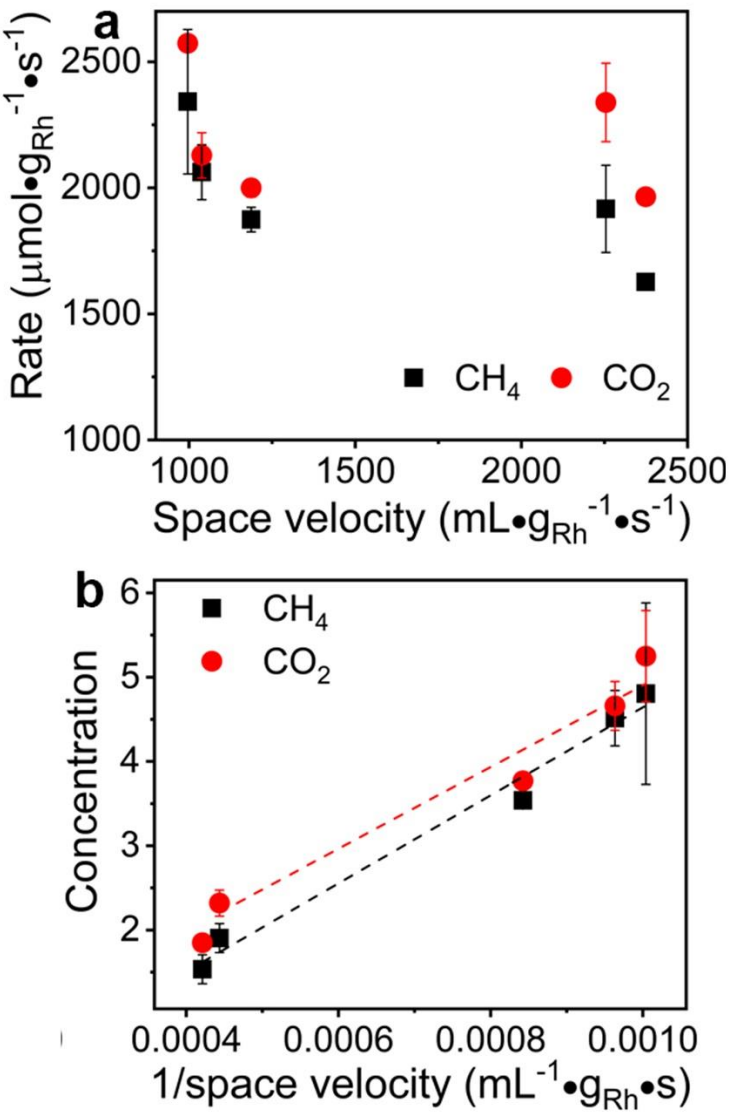

Figure S19. (a) CH_4 production rate and CO_2 consumption rate as a function of gas space velocity. (b) Concertation of CH_4 and reacted CO_2 in the effluent as a function of the reciprocal space velocity. Internal mass transfer should be neglected since the reaction rates is roughly invariant with the space velocity.